

Driven and active colloids at fluid interfaces

Nicholas G. Chisholm¹ and Kathleen J. Stebe^{1†},

¹Department of Chemical and Biomolecular Engineering, University of Pennsylvania,
Philadelphia, PA 19104, USA

(Received xx; revised xx; accepted xx)

We derive expressions for the leading-order far-field flows generated by mobile colloids trapped at planar fluid-fluid interfaces. We consider both externally driven colloids and active colloids (swimmers) either adjacent to or adhered to the interface. In the latter case, we assume a pinned contact line. The Reynolds and capillary numbers are assumed small, in line with typical colloidal systems involving air- or alkane-aqueous interfaces. At clean (surfactant-free) interfaces, the hydrodynamic modes are essentially a restricted set of the usual Stokes multipoles in a bulk fluid. To leading order, driven colloids simply exert Stokelets parallel to the interface, while active colloids drive different kinds of fluid motion depending on their trapped configuration. We then consider how these modes are altered by the presence of an incompressible surfactant layer, which occurs at high Marangoni numbers. This limiting behavior is typical for colloidal-scale systems at small capillary numbers, even when scant surfactant is present. Compared to a clean interface, we find that incompressibility substantially weakens flow directed normal to the interface. Interestingly, for both driven and active colloids, we find that the leading-order flow normal to the interface is associated with colloid asymmetry with respect to the interfacial plane. Flow parallel to the interface, however, is not weakened. Moreover, surface-viscous stresses, if present, potentially generate very long-ranged flow on the interface itself and into the surrounding fluids. We examine the limiting forms of such flows. Our results have important implications for advective mass transport enhancement near fluid boundaries.

1. Introduction

Fluid-fluid interfaces provide a rich setting for driven and active colloidal systems. Here, a driven colloid moves through a fluid due to external forces or torques, for example, a magnetic bead forced by a magnetic field. Active colloids, on the other hand, self-propel by consuming a fuel source. For example, motile bacteria are active colloids that self-propel by the rotation of one or more flagella. Autophoretic nanorods or Janus particles are other examples of commonly studied active colloids. These catalytic swimmers self-propel via generation of chemical gradients that produce a propulsive layer of apparent fluid slip along the colloid surface.

Past work on colloids adhered to interfaces has focused on their usefulness as Brownian rheological probes when embedded in biological lipid membranes or surfactant monolayers, where colloid motion is, in this case, driven by thermal fluctuations. For example, colloidal probes have been used to measure surface viscosity of a fluid interface as a function of surfactant concentration (Sickert *et al.* 2007). Such measurements require theoretical models of the mobility of the colloid. Saffman & Delbrück (1975) analytically computed the mobility of a flat disk embedded in a viscous, incompressible membrane separating two semi-infinite subphases in the limit of large Boussinesq number, a dimensionless number comparing the membrane viscosity to that of the surrounding

† Email address for correspondence: kstebe@seas.upenn.edu

fluid. This calculation was extended to moderate Boussinesq numbers by Hughes *et al.* (1981) and to subphases of finite depth by Stone & Ajdari (1998). Later theoretical work quantified the response of a linearly viscoelastic membrane to an embedded point force (Levine & MacKintosh 2002). The effects of particle anisotropy have been quantified in the context of the mobility of a needle embedded in an incompressible Langmuir monolayer overlying a fluid of varying depth (Fischer 2004). Finally, the impact of interfacial compressibility and surfactant solubility on the drag on a disk embedded in an interface above a thin film of fluid has also been quantified (Elfring *et al.* 2016). The dynamics of (three-dimensional) colloids that protrude into the surrounding fluid phases has also been characterized. Analytical and numerical analyses of the mobility of spheres (Fischer *et al.* 2006; Pozrikidis 2007; Stone & Masoud 2015; Dörr & Hardt 2015; Dörr *et al.* 2016) and thin filaments (Fischer *et al.* 2006) can be found in the literature for clean and surfactant-laden interfaces in the limit of small capillary number, a dimensionless ratio of characteristic viscous stresses to interfacial tension.

Active colloids are also strongly influenced by fluid interfaces. Motile bacteria have been the focus of much research in this context due to their relevance to human health and the environment. Seminal work by Lauga *et al.* (2006) showed, via a resistive-force theory model, that circular trajectories of *E. coli* swimming near a solid boundary are caused by hydrodynamic interaction with the boundary. Similar results are found for free surfaces (Di Leonardo *et al.* 2011), although the direction of circling is reversed. These theoretical models also predict that there is always an induced velocity toward the boundary, effectively trapping bacterium at the surface. More detailed boundary element simulations have shown the existence of stable trajectories of bacteria near solid boundaries, where the distance from the boundary and curvature of the trajectory reach a steady state (Giacché *et al.* 2010). In contrast, similar calculations show only unstable trajectories for swimmers near free surfaces; the swimmer inevitably crashes into the boundary unless it is initially angled steeply enough away to escape it altogether (Pimponi *et al.* 2016). Finally, Shaik & Ardekani (2017) analytically computed of the motion of a spherical squirmer, a common model for microorganism locomotion, near a weakly deformable interface. Others have investigated motion of autophoretic swimmers at fluid interfaces. Gold-platinum catalytic nanorods are highly motile at aqueous-alkane interfaces, and their rate of rotational diffusion can be used to measure interfacial shear viscosity (Dhar *et al.* 2006). Further experiments have shown that partially-wetted, self-propelled Janus particles at air-water interfaces move along circular trajectories with markedly decreased rotational diffusion as compared to their motion in a bulk fluid (Wang *et al.* 2017). Theoretical analysis has yielded analytical predictions of the linear and angular velocities of an autophoretic sphere straddling a surfactant-free interface with a freely-slipping, 90° contact line (Malgaretti *et al.* 2016). This work has supplied valuable information about the influence of fluid interfaces on active colloid locomotion.

Rather than developing detailed models for specific types of swimmers, an alternative approach is to use far-field models that capture universal features of colloid locomotion. For active colloids, this approach has been used to compute swimming trajectories near solid boundaries (Spagnolie & Lauga 2012) and fluid interfaces Lopez & Lauga (2014). Such methods are accurate when the colloid is separated from the boundary by a few body lengths (Spagnolie & Lauga 2012). Recent work has employed far-field models of active colloids to study trapping of microswimmers near surfactant-laden droplets (Desai *et al.* 2018) and the density distribution of bacteria near fluid interfaces (Ahmadzadegan *et al.* 2019).

While active and driven colloids near boundaries have been the subject of past theoretical analysis, the focus has largely been on computing drag (on driven colloids) or

swimming trajectories (of active colloids) and how they are influenced by the boundary. The actual flows generated by such colloids at interfaces and the implications of these flows have received less attention. Aside from trapping due to hydrodynamic interactions, active colloids may be trapped at fluid interfaces by contact-line pinning, a phenomenon unique to fluid interfaces, in a variety of configurations, greatly affecting their motility and their induced fluid flows. For instance, recent work suggests that contact-line pinning traps *Pseudomonas aeruginosa* in a variety of different and persistent orientations at aqueous-hexadecane interfaces, leading to a distinct motility patterns (Deng *et al.* 2020). Bacteria may also become adhered to passive colloids already attached to the interface, towing them as cargo (Vaccari *et al.* 2018). The hydrodynamic implications of such trapped states have not been discussed.

In this article, we use the multipole expansion method to examine the hydrodynamic modes generated by driven and active colloids at fluid interfaces in a variety of different trapped states. We focus on the modes that dominate in the far field, which may be observable in experiment. We focus on the case where the colloid is physically adhered to a fluid interface with a pinned contact line that constrains its motion. We also consider the case where the colloid is adjacent to the interface but not adhered, as might occur due to hydrodynamic trapping. This article is organized as follows. In section 2, we develop the governing equations for the fluid motion due to colloids at two types of fluid interfaces: a clean, surfactant-free interface and an interface that is rendered incompressible by adsorbed surfactant. In section 3, we develop a reciprocal relation that applies to two fluids in Stokes flow separated by either of these types of interface. In section 4, we develop a multipole expansion appropriate for colloids trapped at a clean interface, and we discuss the leading-order modes that are produced in the driven and active cases. We then compare these results to analogous results at an incompressible interface in section 5. Finally, we conclude in section 6 by discussing the implications of our results and opportunities for future research.

2. Governing equations

2.1. Equations of motion

We consider a colloid adhered to a planar interface between two immiscible Newtonian fluids of viscosities μ_1 and μ_2 , which are quiescent in the far field and together form an unbounded domain. We assume the resulting three-phase contact line is pinned, that is, it cannot move relative to the surface of the colloid. For simplicity, we further assume that the interface is flat and lies on the $z = 0$ plane. The physical requirements for the assumption of a flat interface to hold are that (i) viscous stress due to flows generated by the particle are negligible compared to surface tension γ , which determines the equilibrium shape of the interface; (ii) the weight mg of the colloid is also negligible compared to surface tension; and (iii) undulations in the contact line are negligibly small compared to the size of the colloid. Requirement (i) is formally satisfied when $Ca = \mu U / \gamma \ll 1$, where Ca is the capillary number, μ is the fluid viscosity and U is the characteristic velocity of the colloid. For typical colloidal systems at air-aqueous or alkane-aqueous interfaces, $Ca = O(10^{-7})$ to $O(10^{-5})$. Requirement (ii) is satisfied when $Bo = mgl^2 / \gamma \ll 1$, where Bo is the particle Bond number and l is the characteristic length scale of the colloid. Requirement (iii) may not be generally satisfied. For isolated passive particles, nanometric contact line distortions alter the capillary energy that traps colloids on interfaces (Stamou *et al.* 2000), and thermally activated fluctuations at the contact line are hypothesized to alter dissipation in the interface (Boniello *et al.* 2015).

Neither effect is included here, but the results we present may form the basis for a perturbative method to treat the problem of undulated contact lines.

At the colloidal scale, we may neglect the effects of fluid inertia and assume the flow on either side of the interface is governed by the Stokes equations,

$$\nabla \cdot \boldsymbol{\sigma} = -\nabla p + \mu \nabla^2 \mathbf{u} = \mathbf{0}; \quad \nabla \cdot \mathbf{u} = 0, \quad (2.1)$$

subject to the appropriate boundary conditions on the colloid surface, where $\boldsymbol{\sigma} = -p\mathbf{I} + \mu[\nabla \mathbf{u} + (\nabla \mathbf{u})^\top]$ is the stress tensor, \mathbf{I} is the identity tensor, $\mathbf{u} = \mathbf{u}(\mathbf{x})$ is the fluid velocity, $p = p(\mathbf{x})$ is the hydrodynamic pressure, $\mathbf{x} = (x, y, z)$ is the position vector, and ∇ is the gradient operator with respect to \mathbf{x} . Let V_1 , V_2 , and I denote the set of points in fluid 1, fluid 2, and on the interface, respectively. We assume that the viscosity changes abruptly across the interface as $\mu(z) = \mu_1 \mathbb{I}_{z>0}(z) + \mu_2 \mathbb{I}_{z<0}(z)$, where the indicator function $\mathbb{I}_P(z)$ is unity if condition P is satisfied by its argument but otherwise vanishes. We further assume that fluid velocity is continuous across the fluid interface, that is, $[\mathbf{u}]_I = \mathbf{0}$, where $[q_*]_I(\mathbf{x}) = (\lim_{z \rightarrow 0^+} - \lim_{z \rightarrow 0^-})q_*(\mathbf{x})$ denotes the jump in quantity q_* across the interface going from fluid 2 to fluid 1. The general tangential stress balance on the fluid interface is

$$\nabla_s \cdot \boldsymbol{\varsigma} + \mathbf{n} \cdot [\boldsymbol{\sigma}]_I \cdot \mathbf{l}_s = \mathbf{0} \quad (2.2)$$

where $\boldsymbol{\varsigma} = \boldsymbol{\varsigma}(\mathbf{x} \in I)$ is the surface stress tensor, \mathbf{n} is the unit normal to the interface pointing into fluid 1, $\mathbf{l}_s = \mathbf{I} - \mathbf{n}\mathbf{n}$ is the surface projection tensor, and $\nabla_s = \mathbf{l}_s \cdot \nabla$ is the surface gradient operator. The remaining normal component of the interfacial stress balance is replaced by the kinematic condition $\mathbf{u} \cdot \mathbf{n} = 0$ on $z = 0$.

2.2. Clean interface

We call an interface clean if it is free of surfactant molecules. In the absence of temperature gradients, a clean interface is characterized by a uniform surface tension, $\boldsymbol{\varsigma}(\mathbf{x}) = \gamma_0 \mathbf{l}_s$. Then, $\nabla_s \cdot \boldsymbol{\varsigma}$ vanishes and (2.2) reduces to

$$\mathbf{n} \cdot [\boldsymbol{\sigma}]_I \cdot \mathbf{l}_s = \mathbf{0}, \quad (2.3)$$

which states that the tangential stress on the fluid is continuous across the interface.

2.3. Incompressible interface

If surfactant is present, gradients in surfactant concentration due to flow exert Marangoni stresses on the surrounding fluids. At interfaces where $Ca \gg 1$, these gradients need only be infinitesimal to balance viscous stresses due to colloid motion. As a result, the interface is constrained to surface-incompressible motion.

To derive the most conservative estimate for the effects of these Marangoni stresses, consider trace surfactant concentrations, for which the surfactant can be approximated as a two dimensional ideal gas. In this case, the dependence of the surface pressure $\pi = \pi(\mathbf{x} \in I)$ on surfactant concentration $\Gamma = \Gamma(\mathbf{x} \in I)$ is given by $\partial\pi/\partial\Gamma = k_B T$, where k_B is Boltzmann's constant and T is temperature. Scaling the surface pressure by viscous stresses $\tilde{\pi} = \pi/\bar{\mu}U$, where $\bar{\mu} = (\mu_1 + \mu_2)/2$ is the average surface viscosity, and letting $\tilde{\Gamma} = \Gamma/\bar{\Gamma}$, where $\bar{\Gamma}$ is the average surface concentration over the entire interface, we find

$$\tilde{\nabla}_s \tilde{\pi} = \frac{k_B T \bar{\Gamma}}{\bar{\mu}U} \tilde{\nabla}_s \tilde{\Gamma} = Ma \tilde{\nabla}_s \tilde{\Gamma} \quad (2.4)$$

where Ma is the dimensionless Marangoni number and $\tilde{\nabla}_s = l \nabla_s$. To evaluate Ma , we consider typical parameter values for a colloid moving at $U = 10 \mu\text{m/s}$ at a hexadecane-

water interface ($\gamma_0 \approx 50 \text{ mN/m}$) in the surface-gaseous state. The surfactant concentration required to produce a 0.1% decrease in the surface tension is approximately $\bar{\Gamma} = 2 \times 10^3 \text{ molecules}/\mu\text{m}^2$. Given $\bar{\mu} \approx 1 \text{ mPa}\cdot\text{s}$, we estimate that $Ma = O(10^3)$. Thus, very small perturbations in Γ generate sufficient Marangoni stress to balance viscous stresses due to motion of the colloid.

The large Ma limit has the important consequence that the fluid interface behaves as incompressible layer ($\nabla_s \cdot \mathbf{u} = 0$ for $\mathbf{x} \in I$). Assuming bulk-insoluble surfactant, the non-dimensionalized surfactant mass balance on the interface is

$$\tilde{\Gamma}(\mathbf{x}) \tilde{\nabla}_s \cdot \tilde{\mathbf{u}} + Ma^{-1}(\tilde{\mathbf{u}} \cdot \tilde{\nabla}_s) \tilde{\pi} = (Ma Pe)^{-1} \tilde{\nabla}_s^2 \tilde{\pi}, \quad (2.5)$$

where $\tilde{\mathbf{u}} = \mathbf{u}/U$, $Pe = Ul/D_s$ is the Peclet number of the surfactant, and D_s is the surface diffusivity of the adsorbed surfactant. Therefore, (2.5) implies that $\tilde{\nabla}_s \cdot \tilde{\mathbf{u}} \ll 1$ if $Ma \gg 1$ and $Pe_s \gtrsim Ma^{-1}$. Assuming $l = 10 \mu\text{m}$ and $D_s = 10^2 \mu\text{m}^2/\text{s}$ (a typical value for small molecule surfactants), we have $Pe_s = O(1)$, so surfactant diffusion does not typically restore compressibility of the interface. At larger surfactant concentrations, where departure from the surface-gaseous state is expected, the interface will generally remain incompressible because, except during phase transitions, $\partial\gamma/\partial\Gamma > k_B T$. Thus, we hereafter assume $\nabla_s \cdot \mathbf{u} = 0$ while discussing interfaces with surfactant. Dilute soluble surfactants also obey this constraint, as mass transport rates between the bulk and the interface are typically negligible. Here, we note that we may express the Marangoni number as $Ma = E/Ca$, where $E = \partial\tilde{\gamma}/\partial\tilde{\Gamma}$ is the Gibbs elasticity. Thus, interfacial incompressibility is the typical circumstance for any interfacial flow at low capillary number (Bławdziewicz *et al.* 1999).

A separate effect of increased surfactant concentration is the emergence of significant surface-viscous stresses due to interfacial shearing motion. If we assume Newtonian behavior of the surfactant, the interfacial stress tensor can be expressed as

$$\boldsymbol{\varsigma}(\mathbf{x}) = -\pi(\mathbf{x})\mathbf{I}_s + \mu_s \left[\nabla_s \mathbf{u} + (\nabla_s \mathbf{u})^\top \right] \quad (2.6)$$

for $\mathbf{x} \in I$, where μ_s is the surface viscosity. Then, inserting (2.6) into (2.2) yields the tangential stress balance for an incompressible, surfactant-laden interface

$$-\nabla_s \pi + \mu_s \nabla_s^2 \mathbf{u} + \mathbf{n} \cdot [\boldsymbol{\sigma}]_I \cdot \mathbf{I}_s = \mathbf{0}, \quad (2.7)$$

which, in conjunction with the surface incompressibility condition, is analogous to the Stokes equations (if $\mu_s = 0$) for a two dimensional fluid that is forced by viscous stresses from the bulk phases.

3. Reciprocal relation for two fluids separated by an interface

3.1. Lorentz reciprocal theorem across an interface

The Lorentz reciprocal theorem provides a relation between the velocity and stress fields of two arbitrary Stokes flows. We may extend this theorem to two fluid regions separated by a clean or incompressible interface, like those illustrated in figure 1, as follows. Consider a region of fluid $V_\alpha^* \subset V_\alpha$ that is fully contained in fluid α . Let $(\mathbf{u}, \boldsymbol{\sigma})$ and $(\mathbf{u}', \boldsymbol{\sigma}')$ represent the velocity and stress fields of two independent solutions to the Stokes equations (2.1) in V_α^* . Integration of $\nabla \cdot (\boldsymbol{\sigma} \cdot \mathbf{u}' - \boldsymbol{\sigma}' \cdot \mathbf{u})$ over V_α^* and application of the divergence theorem leads to the identity (Kim & Karrila 1991)

$$\int_{V_\alpha^*} [(\nabla \cdot \boldsymbol{\sigma}) \cdot \mathbf{u}' - (\nabla \cdot \boldsymbol{\sigma}') \cdot \mathbf{u}] dV + \int_{\partial V_\alpha^*} (\boldsymbol{\sigma} \cdot \mathbf{u}' - \boldsymbol{\sigma}' \cdot \mathbf{u}) \cdot d\mathbf{S} = 0 \quad (3.1)$$

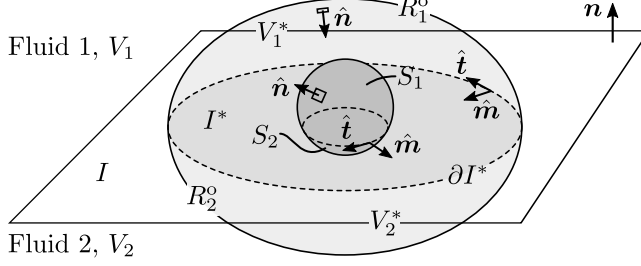


FIGURE 1. A colloid, depicted in the center of the illustration, is surrounded by two arbitrary fluid regions $V_1^* \subset V_1$ and $V_2^* \subset V_2$, which meet at region $I^* \subset I$ on the interface. We assign the inward-facing normal vector $\hat{\mathbf{n}}$ to the boundaries of both of these regions. The unit normal \mathbf{n} (sans hat) of the interface always points in the $+z$ direction. The boundary of V_1^* consists of the colloid surface S_1 , the interfacial region I^* , and the remaining outer surface R_1^o , with the boundaries of V_2^* being similarly labeled. The boundary of I^* (dashed line), denoted ∂I^* , has the counterclockwise oriented tangent vector $\hat{\mathbf{t}}$, and we define $\hat{\mathbf{m}} = \mathbf{n} \times \hat{\mathbf{t}}$, which points into I^* . The three-phase contact line is represented by the inner part of ∂I^* .

where ∂V_α^* denotes the boundary of V_α^* , and $d\mathbf{S} = \hat{\mathbf{n}} dS$ points into ∂V_α^* . If we extend (2.1) to the case where there is an external force density $\mathbf{f}(\mathbf{x})$ on the fluid, then $\nabla \cdot \boldsymbol{\sigma} = -\mathbf{f}(\mathbf{x})$ and $\nabla \cdot \boldsymbol{\sigma}' = -\mathbf{f}'(\mathbf{x})$, which substituted into (3.1) gives the Lorentz reciprocal theorem,

$$\int_{V_\alpha^*} [\mathbf{f}(\mathbf{x}) \cdot \mathbf{u}' - \mathbf{f}'(\mathbf{x}) \cdot \mathbf{u}] dV = \int_{\partial V_\alpha^*} (\boldsymbol{\sigma} \cdot \mathbf{u}' - \boldsymbol{\sigma}' \cdot \mathbf{u}) \cdot d\mathbf{S}. \quad (3.2)$$

If we add the pair of equations given by (3.2) for each of the two fluid phases $\alpha \in \{1, 2\}$, we obtain

$$\begin{aligned} \int_{V^*} [\mathbf{f}(\mathbf{x}) \cdot \mathbf{u}' - \mathbf{f}'(\mathbf{x}) \cdot \mathbf{u}] dV \\ = \oint_R (\boldsymbol{\sigma} \cdot \mathbf{u}' - \boldsymbol{\sigma}' \cdot \mathbf{u}) \cdot d\mathbf{S} + \int_{I^*} ([\boldsymbol{\sigma}]_I \cdot \mathbf{u}' - [\boldsymbol{\sigma}']_I \cdot \mathbf{u}) \cdot \mathbf{n} dA, \end{aligned} \quad (3.3)$$

where $V^* := V_1^* \cup V_2^*$ is the union of the fluid volumes in each phase, $I^* := \partial V_1 \cap \partial V_2$ is the region (at the fluid interface) where V_1^* and V_2^* touch, and $R = \partial V^* \setminus I^*$ constitutes the remaining boundaries of V_1^* and V_2^* that are not adjacent to each other. For example, for the fluid region illustrated in figure 1, $R = S_1 \cup S_2 \cup R_1^o \cup R_2^o$, which includes both the surfaces of the colloid (the inner surfaces of V^*) and the outer surfaces of V^* . In the integral over I^* in (3.3), we have used the fact that the fluid velocity is continuous across the interface, $[\mathbf{u}]_{I^*} = [\mathbf{u}']_{I^*} = \mathbf{0}$. This term can be recast using the interfacial stress balance. Letting \mathbf{t}^* be an arbitrary vector tangent to the interface, (2.2) gives

$$(\nabla_s \cdot \boldsymbol{\varsigma}) \cdot \mathbf{t}^* + \mathbf{n} \cdot [\boldsymbol{\sigma}]_I \cdot \mathbf{t}^* + \mathbf{f}_s \cdot \mathbf{t}^* = 0. \quad (3.4)$$

The final term of this equation accounts for an additional external surface force density $\mathbf{f}_s = \mathbf{f}_s(\mathbf{x} \in I)$ on the interface. Since there is no fluid flux through interface, both \mathbf{u} and \mathbf{u}' are tangent to the interface for $\mathbf{x} \in I$. Thus, using (3.4), (3.3) becomes

$$\begin{aligned} \int_{V^*} [\mathbf{f} \cdot \mathbf{u}' - \mathbf{f}' \cdot \mathbf{u}] dV + \int_{I^*} [\mathbf{f}_s \cdot \mathbf{u}' - \mathbf{f}'_s \cdot \mathbf{u}] dA \\ = \oint_R (\boldsymbol{\sigma} \cdot \mathbf{u}' - \boldsymbol{\sigma}' \cdot \mathbf{u}) \cdot d\mathbf{S} - \int_{I^*} [(\nabla_s \cdot \boldsymbol{\varsigma}) \cdot \mathbf{u}' - (\nabla_s \cdot \boldsymbol{\varsigma}') \cdot \mathbf{u}] dA, \end{aligned} \quad (3.5)$$

where $\boldsymbol{\varsigma}$ and $\boldsymbol{\varsigma}'$ are the interfacial stress tensors associated with the unprimed and primed flows, respectively.

3.2. Clean interface

For a clean interface, $\boldsymbol{\varsigma} = -\mathbf{I}_s \gamma_0$ is constant, so the final integral in (3.5) vanishes;

$$\int_{V^*} [\mathbf{f} \cdot \mathbf{u}' - \mathbf{f}' \cdot \mathbf{u}] dV + \int_{I^*} [\mathbf{f}_s \cdot \mathbf{u}' - \mathbf{f}'_s \cdot \mathbf{u}] dA = \oint_R (\boldsymbol{\sigma} \cdot \mathbf{u}' - \boldsymbol{\sigma}' \cdot \mathbf{u}) \cdot d\mathbf{S}. \quad (3.6)$$

For completeness, we have included the possibility of an external surface force density exerted on the interface itself (even though there is physically no material adhered to it). If we assume $\mathbf{f}_s = \mathbf{f}'_s = \mathbf{0}$, then the integral over I^* in (3.6) also vanishes, which is the same as (3.2) with ∂V_α^* replaced by R .

3.3. Incompressible interface

Assuming an incompressible interface with Newtonian behavior, as described by (2.6), there is a surface reciprocal identity for the interface that is analogous to (3.2) that is given by

$$\int_{I^*} [(\nabla_s \cdot \boldsymbol{\varsigma}) \cdot \mathbf{u}' - (\nabla_s \cdot \boldsymbol{\varsigma}') \cdot \mathbf{u}] dA + \oint_{\partial I^*} (\boldsymbol{\varsigma} \cdot \mathbf{u}' - \boldsymbol{\varsigma}' \cdot \mathbf{u}) \cdot \hat{\mathbf{m}} dC = 0, \quad (3.7)$$

where the final term on the right-hand-side of this equation is a contour integral over the boundary of I^* , denoted ∂I^* . The unit vector $\hat{\mathbf{m}}$ points into I^* , meeting ∂I^* at a right angle. It is defined as $\hat{\mathbf{m}} = \mathbf{n} \times \hat{\mathbf{t}}$, where $\hat{\mathbf{t}}$ is the counterclockwise-oriented unit tangent $\hat{\mathbf{t}}$ vector of ∂I^* (see figure 1). Equation (3.7) in (3.5) yields

$$\begin{aligned} \int_{V^*} [\mathbf{f} \cdot \mathbf{u}' - \mathbf{f}' \cdot \mathbf{u}] dV + \int_{I^*} [\mathbf{f}_s \cdot \mathbf{u}' - \mathbf{f}'_s \cdot \mathbf{u}] dA \\ = \oint_R (\boldsymbol{\sigma} \cdot \mathbf{u}' - \boldsymbol{\sigma}' \cdot \mathbf{u}) \cdot d\mathbf{S} + \oint_{\partial I^*} (\boldsymbol{\varsigma} \cdot \mathbf{u}' - \boldsymbol{\varsigma}' \cdot \mathbf{u}) \cdot \mathbf{m} dC. \end{aligned} \quad (3.8)$$

Comparing (3.8) to the analogous equation for a clean interface (3.6), we see that the final term is new. (3.8) involves a new contour integral over the boundary of I^* . This contour integral over the boundary of I^* accounts for surface pressure gradients, or Marangoni stresses, that enforce the interfacial incompressibility constraint and, if $\mu_s > 0$, for surface-viscous dissipation. While we hereafter restrict ourselves to planar interfaces, we note that (3.6) and (3.8) hold even if the interface is curved, given that it has the same shape in both the primed and unprimed flow problems.

4. Clean fluid interfaces

4.1. Green's function

Due to the linearity of (2.1) and (2.3), we may represent the velocity field due to a point force \mathbf{F} located at $\mathbf{y} = (y_1, y_2, h)$ as $\mathbf{G}(\mathbf{x}, \mathbf{y}) \cdot \mathbf{F}$, where \mathbf{G} is the Green's function for two fluids separated by a clean interface, which satisfies

$$-\nabla P(\mathbf{G}; \mathbf{x}, \mathbf{y}) + \mu(z) \nabla^2 \mathbf{G}(\mathbf{x}, \mathbf{y}) = \begin{cases} \mathbf{0} & h = 0 \\ -\mathbf{I} \delta_{\mathbb{R}^3}(\mathbf{x} - \mathbf{y}) & h \neq 0 \end{cases} \quad (4.1a)$$

$$\nabla \cdot \mathbf{G}(\mathbf{x}, \mathbf{y}) = 0 \quad (4.1b)$$

for $\mathbf{x} \in V_1 \cup V_2$, subject to $|\mathbf{u}| \rightarrow 0$ as $|\mathbf{x}| \rightarrow \infty$ and

$$\mathbf{I}_s \cdot [\mathbf{n} \cdot \mathbf{T}(\mathbf{G}; \mathbf{x}, \mathbf{y})]_I = \begin{cases} -\mathbf{I}_s \delta_{\mathbb{R}^2}(\mathbf{x} - \mathbf{y}) & h = 0 \\ \mathbf{0} & h \neq 0 \end{cases} \quad (4.2a)$$

$$\mathbf{t}^* \cdot [\mathbf{G}(\mathbf{x}, \mathbf{y})]_I = \mathbf{n} \cdot \mathbf{u} = 0 \quad (4.2b)$$

for $\mathbf{x} \in I$. Here, $\mathbf{P}(\mathbf{G};)$ is the (vectorial) pressure field associated with \mathbf{G} , $\mathbf{T}(\mathbf{G};)$ is the stress tensor associated with \mathbf{G} , and $\delta_{\mathbb{R}^n}(\mathbf{x})$ is the Dirac delta in \mathbb{R}^n . Note that for $h = 0$, we take the force as being exerted on the interface itself rather than on one of the fluids.

Solving (4.1) and (4.2a) yields

$$\mathbf{G}(\mathbf{x}, \mathbf{y}) = \begin{cases} [\mathbf{J}(\mathbf{x} - \mathbf{y}) + \mathbf{U}(\mathbf{x}, \mathbf{y}^*)]/\mu(h) & zh \geq 0 \\ \mathbf{V}(\mathbf{x}, \mathbf{y})/\bar{\mu} & zh \leq 0 \\ \mathbf{J}(\mathbf{x} - \mathbf{y}) \cdot \mathbf{I}_s/\bar{\mu} & h = 0, \end{cases} \quad (4.3)$$

where $\mathbf{y}^* = (y_1, y_2, -h)$ is the image reflection of \mathbf{y} through $z = 0$ and $\mathbf{J}(\mathbf{x}) = (\mathbf{I}/r - \mathbf{x}\mathbf{x}/r^3)/8\pi$ is the Oseen tensor. The tensors \mathbf{U} and \mathbf{V} represent hydrodynamic images that are necessary to satisfy continuity of tangential stress (4.2a) and continuity of velocity at the interface. The image systems are given by (Aderogba & Blake 1978)

$$U_{ij}(\mathbf{x}, \boldsymbol{\xi}) = (\delta_{jk}^n - n_j n_k) \left[J_{ik}(\mathbf{x} - \boldsymbol{\xi}) - \frac{\mu(\boldsymbol{\xi} \cdot \mathbf{n})}{\bar{\mu}} V_{ik}(\mathbf{x}, \boldsymbol{\xi}) \right] \quad (4.4)$$

$$V_{ij}(\mathbf{x}, \boldsymbol{\xi}) = \left[\delta_{jk}^n + (\boldsymbol{\xi} \cdot \mathbf{n}) n_k \frac{\partial}{\partial \xi_j} + \frac{1}{2} (\boldsymbol{\xi} \cdot \mathbf{n})^2 \delta_{jk} \frac{\partial^2}{\partial \xi_l^2} \right] J_{ik}(\mathbf{x} - \boldsymbol{\xi}), \quad (4.5)$$

where δ_{jk} is the Kronecker delta and $\delta_{jk}^n = \delta_{jk} - n_j n_k$. The tensor indices $i, j, k, l \in \{1, 2, 3\}$ follow the Einstein summation convention. If, without loss of generality, we assume that the point force at \mathbf{y} is located in the upper fluid ($h > 0$), then a Stokeslet, the Green's function of the Stokes equations in an unbounded fluid, is induced at this point. The flow in the lower fluid ($z < 0$) comprises three image flows: a Stokeslet parallel to the interface, a Stokeslet dipole, and a degenerate Stokes quadrupole (a source doublet), all of which have their singular points at \mathbf{y} (outside the physical domain of the lower fluid). These images correspond to each of the terms in (4.5), respectively. The image system for the upper fluid (4.4) is similar except that the image singularities are located at the image point \mathbf{y}^* . The image system \mathbf{U} also includes an additional image Stokeslet that is the mirror reflection of the original forcing Stokeslet through $z = 0$. Finally, we note that \mathbf{G} is self-adjoint,

$$\mathbf{G}(\mathbf{x}, \mathbf{y}) = \mathbf{G}^\top(\mathbf{y}, \mathbf{x}), \quad (4.6)$$

which may be directly verified from (4.3) or proven using (3.6) (see appendix A). This property will prove useful in the following analysis.

4.2. Multipole expansion

4.2.1. Expansion of the boundary integral equation

Using the Green's function (4.3) as the primed flow field in the reciprocal relation (3.6), we may generate a boundary integral equation for an object at the interface. Consider the interfacially-trapped colloid, illustrated in figure 1, whose upper surface S_1 is in contact with fluid 1 and whose lower surface S_2 is in contact with fluid 2. An arbitrary volume of fluid $V^* = V_1^* \cup V_2^*$ surrounds the colloid, which is bounded by S_1 and S_2 as well as the outer fluid surfaces R_1^o and R_2^o . Using \mathbf{y} as the variable of integration, we make the following substitutions into (3.6): $\mathbf{u}'(\mathbf{y}) \rightarrow \mathbf{G}(\mathbf{y}, \mathbf{x})$, $\boldsymbol{\sigma}'(\mathbf{y}) \rightarrow \mathbf{T}(\mathbf{G}; \mathbf{y}, \mathbf{x})$,

$\mathbf{f}' \rightarrow \mathbf{l}\delta_{\mathbb{R}^3}(\mathbf{y}-\mathbf{x})$, and $\mathbf{f}'_s \rightarrow \mathbf{l}\delta_{\mathbb{R}^2}(\mathbf{y}-\mathbf{x})$. We also assume that the external force densities vanish, $\mathbf{f} = \mathbf{f}_s = \mathbf{0}$. Taking the limit of this equation as the outer surfaces R_1^o and R_2^o are made arbitrarily far from the colloid, we obtain the boundary integral representation of the velocity field,

$$\mathbf{u}(\mathbf{x}) = - \oint_{S_c} \mathbf{G}(\mathbf{x}, \mathbf{y}) \cdot [\boldsymbol{\sigma} \cdot \hat{\mathbf{n}}](\mathbf{y}) dS(\mathbf{y}) + \oint_{S_c} [\mathbf{u}\hat{\mathbf{n}}](\mathbf{y}) \odot \mathbf{T}(\mathbf{G}; \mathbf{y}, \mathbf{x}) dS(\mathbf{y}), \quad (4.7)$$

where $S_c = S_1 \cup S_2$ represents the surface of the colloid and the operator \odot denotes complete contraction of its operands, e.g., $(\mathbf{A} \odot \mathbf{B})_{j_1 \dots j_m} = A_{i_1 \dots i_n} B_{i_n \dots i_1 j_1 \dots j_m}$ if \mathbf{A} is the tensor of lower rank and $(\mathbf{A} \odot \mathbf{B})_{j_1 \dots j_m} = A_{j_1 \dots j_m i_1 \dots i_n} B_{i_n \dots i_1}$ if \mathbf{B} is the tensor of lower rank. Equation (4.7) is clearly similar to the boundary integral equation for external Stokes flows in an unbounded bulk fluid (see, e.g., Kim & Karrila 1991). Indeed, it is derived in an analogous manner using the generalized reciprocal relation (3.6). Integrals over R_1^o and R_2^o vanish because $\mathbf{u} \rightarrow \mathbf{0}$ at points arbitrarily far from the colloid. Moreover, integrals over the interface itself do not appear in (4.7) because \mathbf{G} and \mathbf{T} implicitly account for transmission of hydrodynamic stresses through the interface. Equation (4.7) is valid as long as the volume of the colloid does not change and the colloid does not deform in a manner that would distort the flat shape of the pinned contact line.

To generate a multipole expansion for $\mathbf{u}(\mathbf{x})$, we replace $\mathbf{G}(\mathbf{x}, \mathbf{y})$ and $\mathbf{T}(\mathbf{G}; \mathbf{x}, \mathbf{y})$ in (4.7) with their Taylor series in \mathbf{y} about an point on the interface as near as possible to the center of the colloid, which we designate as the origin $\mathbf{0}$. This process is slightly complicated by the piecewise nature of \mathbf{G} as \mathbf{y} passes from one side of the interface to the other. In particular, certain components of $\nabla_{\mathbf{y}} \mathbf{G}(\mathbf{x}, \mathbf{y})$ contain a jump discontinuity over the interface at $z = 0$. This difficulty is overcome by separating each integral in (4.7) into one over S_1 and another over S_2 , so that the integrand is continuous over each surface of integration. Letting $\mathbf{u}^{(1)}$ and $\mathbf{u}^{(2)}$ denote the contributions from integration over S_1 and S_2 , respectively, we may write the expansion as $\mathbf{u}(\mathbf{x}) = \mathbf{u}^{(1)} + \mathbf{u}^{(2)}$, where

$$\begin{aligned} \mathbf{u}^{(1)}(\mathbf{x}) = & - \sum_{n=0}^{\infty} \frac{1}{n!} \left(\int_{S_1} [\hat{\mathbf{n}} \cdot \boldsymbol{\sigma}](\mathbf{y}) \mathbf{y}^{\otimes n} dS(\mathbf{y}) \right) \odot \left(\lim_{\mathbf{y} \rightarrow \mathbf{0}^+} \nabla_{\mathbf{y}}^{\otimes n} \mathbf{G}^{\top}(\mathbf{x}, \mathbf{y}) \right) \\ & + \sum_{n=0}^{\infty} \frac{1}{n!} \left(\int_{S_1} [\mathbf{u}\hat{\mathbf{n}}](\mathbf{y}) \mathbf{y}^{\otimes n} dS(\mathbf{y}) \right) \odot \left(\lim_{\mathbf{y} \rightarrow \mathbf{0}^+} \nabla_{\mathbf{y}}^{\otimes n} \mathbf{T}(\mathbf{G}; \mathbf{y}, \mathbf{x}) \right) \end{aligned} \quad (4.8)$$

and

$$\begin{aligned} \mathbf{u}^{(2)}(\mathbf{x}) = & - \sum_{n=0}^{\infty} \frac{1}{n!} \left(\int_{S_2} [\hat{\mathbf{n}} \cdot \boldsymbol{\sigma}](\mathbf{y}) \mathbf{y}^{\otimes n} dS(\mathbf{y}) \right) \odot \left(\lim_{\mathbf{y} \rightarrow \mathbf{0}^-} \nabla_{\mathbf{y}}^{\otimes n} \mathbf{G}^{\top}(\mathbf{x}, \mathbf{y}) \right) \\ & + \sum_{n=0}^{\infty} \frac{1}{n!} \left(\int_{S_2} [\mathbf{u}\hat{\mathbf{n}}](\mathbf{y}) \mathbf{y}^{\otimes n} dS(\mathbf{y}) \right) \odot \left(\lim_{\mathbf{y} \rightarrow \mathbf{0}^-} \nabla_{\mathbf{y}}^{\otimes n} \mathbf{T}(\mathbf{G}; \mathbf{y}, \mathbf{x}) \right) \end{aligned} \quad (4.9)$$

Here, $\mathbf{y}^{\otimes n} = \mathbf{y}\mathbf{y} \dots$ (n times) denotes the n -fold tensor product and $\nabla_{\mathbf{y}}^{\otimes n}$ similarly denotes the n -fold gradient operator. Writing \mathbf{T} in terms of \mathbf{G} as

$$T_{ijk}(\mathbf{G}; \mathbf{y}, \mathbf{x}) = \delta_{ij} P_k(\mathbf{G}; \mathbf{y}, \mathbf{x}) + \mu(h) \left(\frac{\partial G_{kj}(\mathbf{x}, \mathbf{y})}{\partial y_i} + \frac{\partial G_{ki}(\mathbf{x}, \mathbf{y})}{\partial y_j} \right)$$

and collecting terms in \mathbf{G} , $\nabla_{\mathbf{y}} \mathbf{G}$, and so on for higher order gradients of \mathbf{G} , we arrive at the multipole expansion,

$$\mathbf{u}(\mathbf{x}) = \mathbf{u}^{m0}(\mathbf{x}) + \mathbf{u}^{m1}(\mathbf{x}) + \mathbf{u}^{m2}(\mathbf{x}) + \text{h.o.t.}, \quad (4.10)$$

where \mathbf{u}^{m0} is the force monopole (zeroth) moment, \mathbf{u}^{m1} is the force dipole (first) moment,

$\mathbf{u}^{\text{m}2}$ is the quadrupole (second) moment, and so on for higher order terms (h.o.t.). In particular, these first three moments are given by

$$u_i^{\text{m}0}(\mathbf{x}) = F_i^{(1)} G_{ij}(\mathbf{x}, \mathbf{0}^+) + F_i^{(2)} G_{ij}(\mathbf{x}, \mathbf{0}^-) \quad (4.10a)$$

$$u_i^{\text{m}1}(\mathbf{x}) = D_{jk}^{(1)} \frac{\partial G_{ij}}{\partial y_k}(\mathbf{x}, \mathbf{0}^+) + D_{jk}^{(2)} \frac{\partial G_{ij}}{\partial y_k}(\mathbf{x}, \mathbf{0}^-) \quad (4.10b)$$

$$u_i^{\text{m}2}(\mathbf{x}) = Q_{jkl}^{(1)} \frac{\partial G_{ij}}{\partial y_l \partial y_k}(\mathbf{x}, \mathbf{0}^+) + Q_{jkl}^{(2)} \frac{\partial G_{ij}}{\partial y_l \partial y_k}(\mathbf{x}, \mathbf{0}^-), \quad (4.10c)$$

where $\mathbf{F}^{(\nu)}$, $\mathbf{D}^{(\nu)}$, and $\mathbf{Q}^{(\nu)}$ are the monopole, dipole, and quadrupole coefficients for fluid $\nu \in \{1, 2\}$, respectively. The shorthand notation $\mathbf{0}^+$ indicates the limit as \mathbf{y} approaches $\mathbf{0}$ from above the interface (i.e., from fluid 1). Similarly, $\mathbf{0}^-$ indicates the limit as \mathbf{y} approaches $\mathbf{0}$ from below. Note that if the colloid is wholly immersed in one fluid, then the multipole coefficients for the other fluid vanish.

At distances, far enough from the colloid that points on the colloid surface are virtually indistinguishable from $\mathbf{0}$, $|\mathbf{x}| \gg l$, the leading terms of (4.10) closely approximate $\mathbf{u}(\mathbf{x})$. The reason is that, at points $|\mathbf{x}| \gg |\mathbf{y}|$, $\mathbf{G}(\mathbf{x}, \mathbf{y})$ effectively appears as a Stokeslet and decays as $|\mathbf{x} - \mathbf{y}|^{-1}$; the image Stokes dipole and degenerate quadrupole terms contained in \mathbf{U} and \mathbf{V} in (4.3) do not affect the far-field behavior of \mathbf{G} because they decay more quickly than the Stokeslet terms. It follows that $\mathbf{u}^{\text{m}0}(\mathbf{x}) \sim r^{-1}$, where $r = |\mathbf{x}|$. Each successive multipole moment involves a higher-order gradient of \mathbf{G} . Thus, $\mathbf{u}^{\text{m}1}(\mathbf{x}) \sim r^{-2}$, $\mathbf{u}^{\text{m}2}(\mathbf{x}) \sim r^{-3}$ and so on for higher-order moments. The lowest order term with a nonzero coefficient dominates the far-field flow. This behavior is analogous to that of the multipole expansion for objects in a bulk fluid.

4.2.2. Monopole moment

The monopole moment corresponds to a point force exerted at the interface, which follows intuitively from the fact that at large distances $r \gg l$, the colloid is indistinguishable from a single point at the interface. The functional form of the flow is therefore just that of the Green's function \mathbf{G} . The prefactors appearing in (4.10a) are given by

$$\mathbf{F}^{(\alpha)} = - \int_{S_\alpha} \boldsymbol{\sigma} \cdot \hat{\mathbf{n}} \, dS, \quad (4.11)$$

which is the force exerted on fluid $\alpha \in \{1, 2\}$ due to motion of the colloid. There is no need to keep the separate limits on the right-hand side of (4.10a) because $\mathbf{G}(\mathbf{x}, \mathbf{y})$ is continuous as \mathbf{y} is moved across the interface for fixed \mathbf{x} . This property is not immediately obvious given the potential viscosity difference between the fluids. Recall, however, the boundary condition (4.2b) that demands continuity of \mathbf{G} as \mathbf{x} is brought across the interface for fixed \mathbf{y} . Since \mathbf{G} is also self-adjoint (4.6), \mathbf{x} implies continuity in \mathbf{y} . Indeed, one may verify directly that all three cases in (4.3) are redundant; the first two cases of this equation reduce to the last as $h \rightarrow 0^\pm$.

Equation (4.3) in (4.10a) yields the monopole moment as

$$u_i^{\text{m}0}(\mathbf{x}) = \frac{1}{\bar{\mu}} F_k \delta_{kj}^n J_{ij}(\mathbf{x}), \quad (4.12)$$

where $\mathbf{F} = \mathbf{F}^{(1)} + \mathbf{F}^{(2)}$ is the total force exerted on both fluids. Equation (4.12) shows that $\mathbf{u}^{\text{m}0}$ is indistinguishable from a Stokeslet in an unbounded fluid of viscosity $\bar{\mu}$ associated with the effective force $\mathbf{F} \cdot \mathbf{l}_s$. The component of \mathbf{F} normal to the interface does not contribute to the flow at leading order due to the presence of the interface. The viscosity-averaged Stokeslet represented by (4.12) possesses an axis of symmetry lying in the

interfacial plane. The tangential shear stress therefore vanishes at $z = 0$, and (2.3) is trivially satisfied. More generally, we will find that any mode with mirror symmetry of the velocity field about the interfacial plane has this property and is therefore a viscosity-averaged flow.

4.2.3. Dipole moment

The functional form of the dipole moment is given by $\nabla_{\mathbf{y}} \mathbf{G}(\mathbf{x}, \mathbf{y})$ in the limit that \mathbf{y} approaches the interface. Thus, this mode corresponds to the flow generated by a pair of opposite point forces at the interface that are displaced by an infinitesimal distance, or, more generally, a linear combination of such force doublets. Its prefactor for phase ν is given by

$$\mathbf{D}^{(\nu)} = \int_{S_\nu} [-(\boldsymbol{\sigma} \cdot \hat{\mathbf{n}})\mathbf{y} + \mu_\nu(\mathbf{u}\hat{\mathbf{n}} + \hat{\mathbf{n}}\mathbf{u})] dS(\mathbf{y}), \quad (4.13)$$

which we decompose as

$$D_{jk}^{(\nu)} = S_{jk}^{(\nu)} + \frac{1}{2}\varepsilon_{jkl}L_l^{(\nu)} + \frac{1}{3}D_{ii}^{(\nu)}\delta_{jk} \quad (4.14)$$

where ε is the permutation tensor. Here, the irreducible tensor $S_{jk}^{(\nu)} = \frac{1}{2}(D_{jk}^{(\nu)} + D_{kj}^{(\nu)}) - \frac{1}{3}D_{ii}^{(\nu)}\delta_{jk}$ is associated with extensional (or contractile) stresses on the fluid, i.e., the stresslet at the interface, and $\mathbf{L}^{(\nu)}$ gives the torque exerted by the colloid on fluid ν ,

$$\mathbf{L}^{(\nu)} = \boldsymbol{\varepsilon} : \mathbf{D}^{(\nu)} = - \int_{S_\nu} \mathbf{y} \times (\boldsymbol{\sigma} \cdot \hat{\mathbf{n}}) dS(\mathbf{y}), \quad (4.15)$$

and $\mathbf{L} = \mathbf{L}^{(1)} + \mathbf{L}^{(2)}$ is the total hydrodynamic torque on the system. The last term of (4.14) is associated with an isotropic stress, which does not produce flow due to fluid incompressibility (4.1b). Thus, it makes no contribution to \mathbf{u}^{m1} .

We may rewrite (4.10b) as

$$\begin{aligned} u_i^{\text{m1}}(\mathbf{x}) = & (D_{\alpha\beta}^{(1)} + D_{\alpha\beta}^{(2)}) \frac{\partial G_{i\alpha}}{\partial y_\beta}(\mathbf{x}, \mathbf{0}) + D_{\alpha 3}^{(1)} \frac{\partial G_{i\alpha}}{\partial y_3}(\mathbf{x}, \mathbf{0}^+) + D_{\alpha 3}^{(2)} \frac{\partial G_{i\alpha}}{\partial y_3}(\mathbf{x}, \mathbf{0}^-) \\ & + \left(D_{3\beta}^{(1)} + D_{3\beta}^{(2)} \right) \frac{\partial G_{i3}}{\partial y_\beta}(\mathbf{x}, \mathbf{0}) + \left(D_{33}^{(1)} + D_{33}^{(2)} \right) \frac{\partial G_{i3}}{\partial y_3}(\mathbf{x}, \mathbf{0}) \end{aligned} \quad (4.16)$$

where we introduce the convention that Greek tensor subscripts, here $\alpha \in \{1, 2\}$ and $\beta \in \{1, 2\}$, only run over the axes parallel to the interface. We have combined the separate limits in the first and penultimate terms of (4.16) because gradients of \mathbf{G} parallel to the interface are continuous. Furthermore, the same penultimate term vanishes; as we can see from (4.3), G_{i3} vanishes at all points on the interface for $\mathbf{y} = \mathbf{0}$. We have also combined the limits in the final term of (4.16) since

$$0 = \left[\frac{\partial G_{\alpha i}(\mathbf{y}, \mathbf{x})}{\partial y_\alpha} \right]_I = \left[\frac{\partial G_{3i}(\mathbf{y}, \mathbf{x})}{\partial y_\alpha} \right]_I = \left[\frac{\partial G_{i3}(\mathbf{x}, \mathbf{y})}{\partial y_3} \right]_I. \quad (4.17)$$

The first equality follows from continuity of parallel gradients, the second from (4.1b) and the third from (4.6). Note that the first two equalities swap the usual roles of \mathbf{x} and \mathbf{y} . Finally, we must maintain the limits on the second and third terms of (4.16) because $[\partial G_{i\alpha}/\partial y_3]_I \neq 0$. The tangential stress balance on the interface (4.2a) requires that

$$\mu_1 \lim_{\mathbf{x} \rightarrow \mathbf{0}^+} \frac{\partial G_{\alpha k}(\mathbf{x}, \mathbf{y})}{\partial x_3} - \mu_2 \lim_{\mathbf{x} \rightarrow \mathbf{0}^-} \frac{\partial G_{\alpha k}(\mathbf{x}, \mathbf{y})}{\partial x_3} = 0. \quad (4.18)$$

Therefore, applying (4.6) to (4.18), we find that the jump in $\partial G_{i\alpha}(\mathbf{x}, \mathbf{y})/\partial y_3$ is by a factor of the viscosity ratio as \mathbf{y} is moved across the interface for fixed \mathbf{x} .

Putting (4.14) in (4.16) and evaluating the necessary components of $\nabla_{\mathbf{y}} \mathbf{G}$, we may express the dipole moment explicitly in terms of the gradient of the Oseen tensor as

$$u_i^{m1}(\mathbf{x}) = -\frac{1}{\bar{\mu}} \left[S_{jk}^{\parallel} + S^{\perp} n_j n_k + \frac{1}{2} \varepsilon_{jk3} L_3 + \frac{\mu(-z)}{\mu_1} A_{jk}^{(1)} + \frac{\mu(-z)}{\mu_2} A_{jk}^{(2)} \right] \frac{\partial J_{ij}(\mathbf{x})}{\partial x_k}, \quad (4.19)$$

where

$$S_{jk}^{\parallel} = \left(\delta_{j\alpha}^{\parallel} \delta_{k\beta}^{\parallel} - \frac{1}{2} \delta_{jk}^{\parallel} \delta_{\alpha\beta}^{\parallel} \right) (S_{\alpha\beta}^{(1)} + S_{\alpha\beta}^{(2)}) \quad (4.20)$$

$$S^{\perp} = S_{33}^{(1)} + S_{33}^{(2)} = -\delta_{\alpha\beta}^{\parallel} (S_{\alpha\beta}^{(1)} + S_{\alpha\beta}^{(2)}) \quad (4.21)$$

$$A_{jk}^{(\nu)} = (\delta_{j\alpha}^{\parallel} n_k + n_j \delta_{k\alpha}^{\parallel}) \left(S_{\alpha 3}^{(\nu)} - \frac{1}{2} \varepsilon_{3\alpha\beta} L_{\beta}^{(\nu)} \right). \quad (4.22)$$

Each of the bracketed coefficients on the right-hand side of (4.19) make distinct contributions to the dipole moment at the interface. The first coefficient \mathbf{S}^{\parallel} , given by (4.20), is a viscosity-averaged stresslet associated with extensional stresses produced by the colloid in the interfacial plane. Similarly, the second coefficient S^{\perp} , given by (4.21), is the viscosity-averaged stresslet perpendicular to the interface. Furthermore, $S_{33}^{(\nu)} = -S_{11}^{(\nu)} - S_{22}^{(\nu)}$ because $\mathbf{S}^{(\nu)}$ is traceless, so \mathbf{S}^{\perp} accounts for extensional stress perpendicular to the interface and planar compression of the interface. The third coefficient is a viscosity-averaged rotlet, or point torque, about the z axis of strength L_3 . These viscosity-averaged flows exhibit mirror symmetry of the velocity field about $z = 0$. Therefore, the tangential shear stress due to these modes vanishes on the interface, as is the case for the monopole moment.

From the corresponding terms in (4.19), we see that the contributions to the dipole moment from $\mathbf{A}^{(1)}$ and $\mathbf{A}^{(2)}$ do not produce viscosity-averaged flows. As anticipated, the flow speed in one phase differs from that in the opposite phase by a factor of the viscosity ratio. (Intuitively, the flow is slower in the more viscous phase.) The difference in flow speed and the requirement that $[\mathbf{u}]_I = \mathbf{0}$ necessitates that $\mathbf{u}^{m1}(\mathbf{x} \in I) = \mathbf{0}$. Interestingly, from (4.22), we see that the components of the stresslet $S_{i3}^{(\nu)}$ and torque $L_i^{(\nu)}$ for $i \in \{1, 2\}$ contribute in a degenerate manner to $\mathbf{A}^{(\nu)}$. Although these modes are not viscosity-averaged, we see from (4.19) and (4.22) that the flow in the upper half-space ($z > 0$) of fluid 1 is equivalent to stresslet in an unbounded fluid (of viscosity $\bar{\mu}$), given by $\mathbf{S}_{\text{upper}}^{\text{eff}} = (\mu_2/\mu_1) \mathbf{A}^{(1)} + \mathbf{A}^{(2)}$, with its singular point at $z = 0$. For the lower fluid ($z < 0$), the effective stresslet is similarly $\mathbf{S}_{\text{lower}}^{\text{eff}} = \mathbf{A}^{(1)} + (\mu_1/\mu_2) \mathbf{A}^{(2)}$.

The quadrupolar and higher order moments of (4.10) can be similarly decomposed into two subsets of modes; one whose tangential stress vanishes at the interface and another whose velocity vanishes at the interface. Members of the former subset will be mirror-symmetric, viscosity-averaged flows and the latter will have velocities that differ by in magnitude by the viscosity ratio on either side of the interface. Here, we do not detail the higher-order modes further; the force monopole (4.12) and force dipole (4.19) describe the leading-order flows of driven and active colloids, respectively. Moreover, in many situations, we can infer the leading-order modes of different driven or active colloids in different configurations on or near the interface.

4.3. Discussion

4.3.1. Driven colloids

For colloids driven by an external force \mathbf{F}_{ext} , it is clear that the monopole moment (4.12)—a viscosity averaged Stokeslet—is the leading-order far-field flow, except in the case that this force is exactly perpendicular to the interface, in which case $\mathbf{u}^{\text{m}0}$ vanishes. The force balance parallel to the interface is $\mathbf{F} \cdot \mathbf{l}_s = \mathbf{F}_{\text{ext}} \cdot \mathbf{l}_s$; this relationship holds whether or not the colloid is adhered or adjacent to the interface. For an adhered colloid, a purely perpendicular external force generates no motion because the pinned contact line is fixed on its surface.

Of course, if the colloid is adjacent to the boundary, it may translate perpendicular to the interface, in which case a normal external force is balanced by the z -component of the hydrodynamic drag. For instance, consider the case where the external force $\mathbf{F}_{\text{ext}} = F_3 \hat{\mathbf{z}}$ acts on a colloid immersed completely in fluid 1 that is distance h from the interface. Then, from (4.11), $\mathbf{F}^{(1)} = \mathbf{F} = F_3 \hat{\mathbf{z}}$ and $\mathbf{F}^{(2)} = \mathbf{0}$. The monopole moment $\mathbf{u}^{\text{m}0}$ (4.12) vanishes because $\mathbf{F} \cdot \mathbf{l}_s = \mathbf{0}$. The leading order flow therefore falls to the dipole moment. Recall that we measure $\mathbf{D}^{(1)}$ with respect to a point on the interface ($\mathbf{x} = \mathbf{0}$), while the center of the colloid is located at $\mathbf{x} = h \hat{\mathbf{z}}$. Substituting $\mathbf{y} = h \hat{\mathbf{z}} + \mathbf{y}_c$ in (4.13), where \mathbf{y}_c is the displacement from the center of the colloid, we find

$$\mathbf{D}^{(1)} = - \int_{S_1} (\boldsymbol{\sigma} \cdot \hat{\mathbf{n}})(h \hat{\mathbf{z}} + \mathbf{y}_c) dS(\mathbf{y}_c) = h F_3 \hat{\mathbf{z}} \hat{\mathbf{z}} + \mathbf{D}_c, \quad (4.23)$$

where \mathbf{D}_c is the dipole strength as measured from the colloid center. Thus, the external force on the colloid contributes a factor of $h F_3 \hat{\mathbf{z}} \hat{\mathbf{z}}$ to $\mathbf{D}^{(1)}$ (or a factor of $h F_3$ to S^\perp). When the particle is far from the interface, the contribution from the normal force dominates because $|\mathbf{y}_c| \sim l \ll h$. Otherwise, when $h \sim l$, contributions from \mathbf{D}_c are generally significant and are sensitive to particle geometry, its distance to the interface, and the viscosity ratio.

An external torque \mathbf{L}_{ext} on the colloid also drives flow. We first consider a torque about the z -axis, $\mathbf{L}_{\text{ext}} = L_{\text{ext},z} \hat{\mathbf{z}}$. This torque must be balanced hydrodynamically whether or not the colloid is adhered to the interface, $L_3 = L_{\text{ext},z}$. Note that pinned contact lines do not resist rotation about the z -axis. The torque induces a viscosity-averaged rotlet, given by the third bracketed term in (4.19). For colloids that are axisymmetric about the z -axis, this is the only non-vanishing mode of (4.19); it is readily shown that $S_{jk}^{\text{u}} = S^\perp = A_{jk}^{(\nu)} = 0$ due to the azimuthal symmetry of the resulting flow. Of course, these coefficients are generally nonzero for general colloid geometries, so an external torque potentially produces all of the modes represented by (4.19).

4.3.2. Active colloids

Active colloids self-propel absent external forces or torques. For many kinds of active colloids, self-propulsion is generated by some active, thrust-producing part of the colloid that drives the remaining passive part, as illustrated in figure 2; spatial separation of thrust and drag on the object generate a hydrodynamic dipole. Therefore, in a bulk fluid, an appropriate far-field model of an active colloid is that of a stresslet along the axis of swimming (Lauga & Powers 2009), which gives the velocity field

$$\mathbf{u}^{\text{S}}(\mathbf{e}; \mathbf{x}) = -\frac{D}{\mu_{\text{b}}} \mathbf{e}(\mathbf{e} \cdot \boldsymbol{\nabla}) \mathbf{J}(\mathbf{x}), \quad (4.24)$$

where D is the strength of the force dipole, μ_{b} the viscosity of the bulk fluid, and \mathbf{e} is a unit vector indicating the swimmer alignment. A similar model makes sense for an active

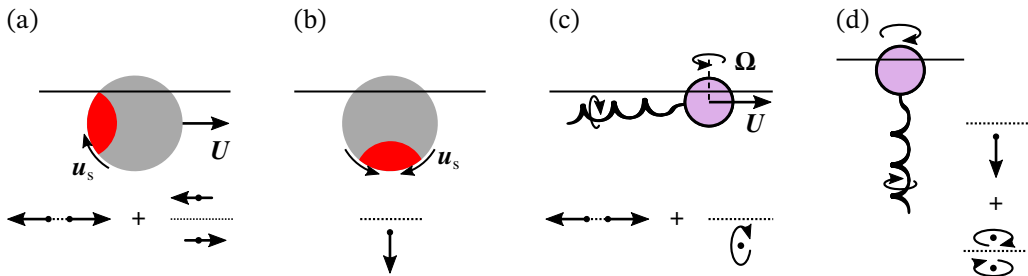


FIGURE 2. Panels (a) and (b) illustrate a phoretic active colloid pinned to the interface. In (a), the active cap of the colloid generates a slip velocity that leads to in-plane swimming of a colloid pinned to the interface at velocity \mathbf{U} . In (b), the colloid active cap instead pumps fluid because contact line pinning prevents forward swimming. Panels (c) and (d) illustrate a bacterium also in swimming and pumping configurations. Thrust is generated by a rotating flagellum, which also produces a torque. In (c), this torque is balanced by capillary pinning, so there is a net hydrodynamic torque exerted on the fluid below the interface. For the vertically adhered bacterium (d), the hydrodynamic torque on the upper and lower fluid must vanish, since the body of the bacteria is free to counterrotate about the z axis. The diagrams next to each illustration give appropriate minimal point-force models that correspond to the leading-order flows they are expected to generate. The arrows represent the orientation of these forces or torques (circular arrows) relative to the interface (dashed line).

colloid swimming parallel to the interface as illustrated in figure 2(a) and (c). Indeed, the same velocity field as (4.24) is produced by setting $\mathbf{S}^{\parallel} = D\mathbf{e}\mathbf{e}/2$ and $S^{\perp} = -D/2$ in (4.19), with $\bar{\mu}$ replacing μ_b . The resulting flow profile is illustrated in figure 3a.

Interestingly, we find a similar mode if we set $S^{\perp} = D$ (with all other coefficients zero) and $\mathbf{e} = \mathbf{n}$ in (4.19). This mode is expected of active colloids trapped perpendicular to the interface as depicted in figure 2(b) and (d). The colloid cannot self-propel in this configuration due to the pinned contact line, so the apparent stresslet (4.24) is not due to balancing hydrodynamic thrust and drag. Instead of swimming, the colloid becomes a fluid pump, resulting in a non-zero net hydrodynamic force on the colloid that is balanced by capillary forces. A minimal model for this pumping configuration is that of a point force exerted along the z -axis a small distance δ from the interface. While the monopole moment vanishes for a force in this direction, the dipole moment does not due to the small but finite separation of the force from the interface. The vertical point force gives $S^{\perp} = F\delta$ in (4.19), which is associated with the flow plotted in figure 3b. Viewed in the interfacial plane, this flow is sink-like for a pusher ($S^{\perp} > 0$) and source-like for a puller ($S^{\perp} < 0$). A pusher causes surface expansion ($\nabla_s \cdot \mathbf{u} > 0$), as new interface must be created to replace the sink. Conversely, a puller causes surface compression.

Another unique feature of active colloids pinned to interfaces is that they may exert an active hydrodynamic torque on the fluid about an axis parallel to the interface. This torque is balanced by surface tension at the pinned contact line. Figure 2c illustrates this scenario for a motile bacterium pinned by its body and propelled by a rotating flagellum. The effect of this torque on the far-field flow enters through $\mathbf{A}^{(1)}$ for a torque on fluid 1 or $\mathbf{A}^{(2)}$ for a torque on fluid 2 (4.22). The resulting flow profile is shown in figure 3c. The presence of this mode potentially discriminates the far-field flow of adhered versus unadhered swimmers; the net torque must vanish for detached active colloids that are adjacent to the interface. In the case of a bacterium, counterrotation of the body and flagellum instead produce a torque dipole in the far-field, a member of the higher-order quadrupole moment. A perpendicular configuration of the bacterium, as in figure 2(d)

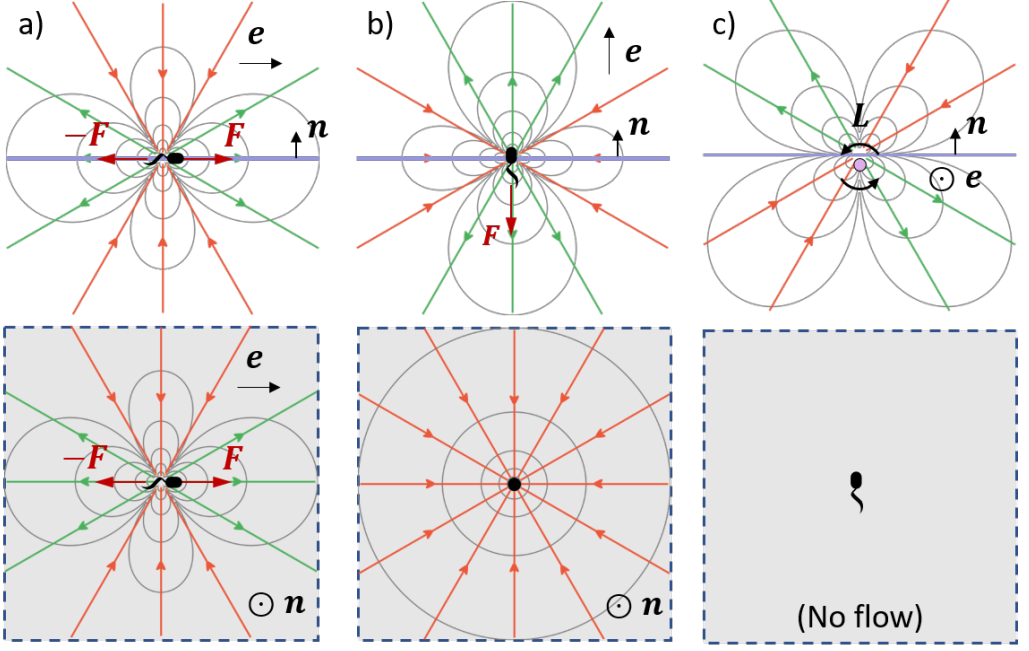


FIGURE 3. Dipolar hydrodynamic modes driven by an active colloid at a clean interface viewed level with the interface (top panels) and on the interfacial plane (bottom panels). The directed lines are streamlines in the laboratory frame and the gray lines are contours of constant flow speed. The vector \mathbf{e} represents the alignment of the swimmer. (a) Force dipole (stresslet) mode expected for a swimmer moving parallel to the interface (pinned or unpinned), viewed along the interface. The configuration of the swimmer is like that in figure 2a or c. (b) Stresslet due to an active colloid pinned at the interface, with a configuration as illustrated in figure 2b or d. Modes (a-b) are the same as the force dipole in a bulk fluid with viscosity $\bar{\mu}$ and are axisymmetric about the swimmer alignment axis indicated by the vector \mathbf{e} . (c) Flow due to a point torque on the fluid where the torque vector \mathbf{L} is parallel to the interface. Such a flow is expected for certain active colloids such as the bacterium illustrated in figure 2c. A degenerate mode is generated by colloids adhered to the interface in an asymmetric manner, e.g., the colloid illustrated in figure 2a.

produces a torque dipole as well because the body may freely counterrotate in the interface.

4.3.3. Symmetry about the interfacial plane

To conclude this discussion, we return to the motif of two major categories of modes: those which are weighted by the average viscosity, with vanishing tangential stress at the interface, and those whose velocity vanishes on the interface. In particular, the subset of dipolar modes corresponding to $\mathbf{A}^{(1)}$ and $\mathbf{A}^{(2)}$ in (4.19) are the only ones that fall into the latter category. The previous discussion associated $\mathbf{A}^{(1)}$ and $\mathbf{A}^{(2)}$ with a net hydrodynamic torque on the fluid adjacent to the interface about an axis parallel to the interface. Such torques might arise from active stresses or, for colloids adjacent to the interface, a driving external torque. However, this mode is not uniquely associated with these torques; from (4.22), we see that it also involves the components of the stresslet $S_{\alpha 3}^{(\nu)}$.

To gain a better understanding of these modes, consider a spherical colloid of radius a driven in rigid-body motion, which is adhered to the interface with a 90° contact angle,

such that half of the sphere is in each fluid. In this case, we may obtain the velocity field from that of a sphere moving in an unbounded fluid of uniform viscosity $\bar{\mu}$ (Ranger 1978; Pozrikidis 2007). If the sphere translates at velocity \mathbf{U} in the $z = 0$ plane and rotates with angular velocity $\hat{\mathbf{t}}_z \Omega_3$, the fluid velocity in the laboratory frame with its origin at the center of the sphere is

$$\mathbf{u}(\mathbf{x}) = \mathbf{F} \left(1 + \frac{a^2}{6} \nabla^2 \right) \cdot \mathbf{J}(\mathbf{x}) + \frac{1}{2} L_3 \hat{\mathbf{t}}_z \cdot [\nabla \times \mathbf{J}(\mathbf{x})], \quad (4.25)$$

where $\mathbf{F} = 6\pi\bar{\mu}\mathbf{U}a$ is the Stokes drag and $L_3 = 8\pi\bar{\mu}\Omega_3$ is the torque. This velocity field is mirror-symmetric about the $z = 0$ plane, so the tangential stress vanishes on $z = 0$. It follows that (4.25) trivially satisfies (2.3) and is therefore also the solution for two fluids of differing viscosities that average to $\bar{\mu}$; the flow is independent of the viscosity contrast. There is, of course, a normal stress jump across the interface in this case, but it is inconsequential at small Ca —the interface remains flat.

Equation (4.25) comprises a viscosity-averaged Stokeslet and degenerate quadrupole (or source doublet) at the center of the sphere. This solution implies that, for the sphere described above, the dipole moment completely vanishes unless there is an external torque about the z -axis, in which we obtain the viscosity-averaged rotlet described by (4.19) and (4.20). If there is no external torque on the sphere but it translates along, e.g., the x axis, then we expect a torque about the y -axis for differing fluid viscosities. One might naively expect this hydrodynamic torque to produce flow, which clearly contributes to $\mathbf{A}^{(\nu)}$ (4.22). However, for a sphere, it is readily shown that the final two bracketed terms of (4.19) cancel.

More generally, we expect a viscosity-averaged flow to result for any driven or active colloid with mirror symmetry about $z = 0$. If the boundary motion is symmetric about $z = 0$, then the resulting fluid flow will reflect this symmetry. By the same arguments for a sphere presented above, identically vanishing tangential stress across the interface implies a viscosity averaged flow. Thus, $\mathbf{A}^{(\nu)}$ and the contribution they make to the dipole moment only contribute to the flow when there is some degree of asymmetry about the interfacial plane. For driven colloids, this asymmetry may come from an asymmetric colloid shape or an adhered configuration that places more of the colloid in one fluid (for a sphere, any contact angle other than 90° will do). For active colloids, there will likely be asymmetry in activity or boundary motion, especially if the two fluid phases have differing viscosities or chemical properties. For example, the phoretic swimmer illustrated in figure 2a is expected to produce a leading-order stresslet parallel to the interface due to hydrodynamic thrust and drag (figure 3a). However, we also expect a contribution from the asymmetric mode illustrated by figure 3c. In experiment, contact line pinning fixes colloids in random configurations at fluid interfaces, so such asymmetric adhered states are likely to be the norm.

5. Incompressible interfaces and the role of surface viscosity

5.1. Green's function

We may define a Green's function \mathbf{H} for an incompressible interface that is analogous to that discussed in section 4.1 for a clean interface. The major difference is that the

interfacial stress balance (4.2a) is replaced by

$$-\nabla_s \Pi(\mathbf{H};) + \mu_s \nabla_s^2 \mathbf{H} + \mathbf{I}_s \cdot [\mathbf{n} \cdot \mathbf{T}(\mathbf{H};)]_I = \begin{cases} -\mathbf{I}_s \delta_{\mathbb{R}^2}(\mathbf{x} - \mathbf{y}) & h = 0 \\ \mathbf{0} & h \neq 0 \end{cases} \quad (5.1a)$$

$$\nabla_s \cdot \mathbf{H} = 0, \quad (5.1b)$$

where $\Pi(\mathbf{H};)$ is the (vectorial) surface pressure associated with \mathbf{H} , which enforces the surface incompressibility constraint (5.1b). Thus, \mathbf{H} satisfies (4.1) subject to (4.2b) and (5.1), with \mathbf{G} replaced by \mathbf{H} in the former two equations. Like \mathbf{G} , \mathbf{H} is self-adjoint (see appendix A);

$$\mathbf{H}(\mathbf{x}, \mathbf{y}) = \mathbf{H}^\top(\mathbf{y}, \mathbf{x}). \quad (5.2)$$

The functional form of \mathbf{H} , given by (Bławdziewicz *et al.* 1999), is more complicated than that of \mathbf{G} owing to the more complex interfacial mechanics. Interestingly, to determine the leading-order moments for colloids at interfaces, it suffices to know \mathbf{G} and $\mathbf{H}(\mathbf{x}, \mathbf{y})$ for $\mathbf{y} \in I$ only, that is, the flow due to a point force at the incompressible interface ($h = 0$). The relevant derivations are outlined in appendix B. Letting $\mathbf{H}^0(\mathbf{x}) = \mathbf{H}(\mathbf{x}, \mathbf{0})$ and $\mathbf{s} = (x, y)$, we find that

$$H_{\alpha\beta}^0(L_B; \mathbf{x}) = \frac{1}{4\pi\bar{\mu}} R_0(L_B; s, z) \delta_{\alpha\beta} + \frac{1}{2\pi\bar{\mu}} R_2(L_B; s, z) \{\hat{s}_\alpha \hat{s}_\beta\}_0 \quad (5.3)$$

and that $H_{3j}^0 = H_{i3}^0 = 0$, where $\hat{\mathbf{s}} = |\mathbf{s}|/s$ and $\{\cdot\}_0$ denotes the irreducible (traceless, symmetric) part of the enclosed tensor. Here, $\{\hat{s}_\alpha \hat{s}_\beta\}_0 = \hat{s}_\alpha \hat{s}_\beta - \frac{1}{2} \delta_{\alpha\beta}$. (Note that we regard this operation is being on a two-dimensional vector since $\alpha, \beta = \{1, 2\}$.) The functions R_0 and R_2 , given by (B 15), depend on the Boussinesq length, $L_B = \mu_s/\bar{\mu}$, as well as position.

The velocity field represented by \mathbf{H}^0 is everywhere parallel to the interface. As noted by Stone & Masoud (2015), this result holds generally for Stokes flows driven by arbitrary incompressible surface motion. The z component of the velocity vanishes on the interface as does its derivative in the z direction; $[\partial u_3/\partial x_3]_{z=0} = -\nabla_s \cdot \mathbf{u} = 0$ because $\nabla \cdot \mathbf{u} = 0$. The z velocity and all its derivatives also vanish at infinity. As a Stokes flow, \mathbf{u} is also biharmonic, $\nabla^4 u_3 = 0$, but, due to its homogeneous behavior of u_3 at the boundaries, u_3 is just the trivial solution to this equation and $u_3 = 0$ everywhere. The vanishing behavior of H_{3j} reflects this fact.

At distances $r \gg L_B$, bulk viscous effects dominate over surface viscous effects. If L_B is vanishingly small compared to the length scale of the colloid l , then surface-viscous effects are negligible, and the flow is only modified from that at a clean interface by Marangoni stresses. Thus, we define the dimensionless Boussinesq number as $Bq = L_B/l$, which quantifies the relative importance of surface viscous to bulk viscous effects. In the limit $Bq \rightarrow 0$, we obtain R_n in closed form (B 16), and (5.3) reduces to

$$H_{\alpha\beta}^0|_{Bq=0} = \frac{\delta_{\alpha\beta}}{8\pi\bar{\mu}r} + \frac{(r - |z|)^2}{4\pi\bar{\mu}rs^2} \{\hat{s}_\alpha \hat{s}_\beta\}_0. \quad (5.4)$$

Marangoni stresses do not affect the rate of decay of the flow from the origin, which remains as r^{-1} . The flow on the interface is purely radial (although not radially symmetric), and is given by

$$H_{\alpha\beta}^0(\mathbf{x} \in I)|_{Bq=0} = \frac{\delta_{\alpha\beta}}{8\pi\bar{\mu}r} \hat{s}_\alpha \hat{s}_\beta. \quad (5.5)$$

In the opposite limit, $Bq \gg 1$, surface viscosity has a dominant impact on the flow at distances $r \ll L_B$. Here, bulk viscous stresses from the surrounding fluid are very weak

compared the interfacial stresses. Then, from (5.1), we recover the equations governing a two-dimensional Stokes flow (Saffman & Delbrück 1975). Therefore, at distances $r \ll L_B$ from the colloid,

$$H_{\alpha\beta}^0|_{Bq \rightarrow \infty} \sim \frac{\hat{s}_\alpha \hat{s}_\beta - \delta_{\alpha\beta} \ln s}{4\pi\mu_s}, \quad (5.6)$$

which is constant in z (it is a two-dimensional flow field) and diverges logarithmically as s is made large. Clearly, (5.6) cannot satisfy the homogenous boundary conditions at $r \rightarrow \infty$. Of course, this is Stokes' paradox, and it is resolved by noting that (5.6) is not valid for $r \gtrsim L_B$, where bulk viscous effects inevitably become important. Despite the rather complicated form of R_n for finite Bq , its main role is simply to transition the flow field between the surface-viscosity-dominated, non-convergent behavior at distances $r \ll L_B$ from the colloid to the convergent, $1/r$ decay at distances $r \gg L_B$, where surface viscosity has a negligible effect. Interestingly, the surface pressure associated with \mathbf{H}^0 is independent of L_B and is given quite simply by $\Pi^0 = s/4\pi s^2$.

5.2. Multipole expansion

5.2.1. Expansion of the boundary integral equation

Using the reciprocal relation (3.8) for two fluids separated by an incompressible interface and following a procedure similar to that described in section 4.2.1, we obtain the boundary integral representation for $\mathbf{u}(\mathbf{x})$ as

$$\begin{aligned} u_k(\mathbf{x}) = & - \oint_{S_c} H_{kj}(\mathbf{x}, \mathbf{y})(\hat{n}_i \sigma_{ij})(\mathbf{y}) dS(\mathbf{y}) + \oint_{S_c} (\hat{n}_i u_j)(\mathbf{y}) T_{ijk}(\mathbf{H}; \mathbf{y}, \mathbf{x}) dS(\mathbf{y}) \\ & - \oint_C H_{k\beta}(\mathbf{x}, \mathbf{y})(\hat{m}_\alpha \varsigma_{\alpha\beta})(\mathbf{y}) dC(\mathbf{y}) + \oint_C (\hat{m}_\alpha u_\beta)(\mathbf{y}) \Sigma_{\alpha\beta k}(\mathbf{H}; \mathbf{y}, \mathbf{x}) dC(\mathbf{y}), \end{aligned} \quad (5.7)$$

for $\alpha, \beta, \gamma \in \{1, 2\}$, where $\hat{\mathbf{m}} = \hat{\mathbf{i}}_z \times \hat{\mathbf{t}}$, C is the curve in the $z = 0$ plane that runs along the three-phase contact line, and $\Sigma(\mathbf{H};)$ is the surface stress tensor associated with \mathbf{H} , which is given by

$$\Sigma_{\alpha\beta k}(\mathbf{H}; \mathbf{y}, \mathbf{x}) = -\delta_{\alpha\beta} \Pi_k(\mathbf{H}; \mathbf{y}, \mathbf{x}) + \mu(h) \left(\frac{\partial H_{k\beta}(\mathbf{x}, \mathbf{y})}{\partial y_\alpha} + \frac{\partial H_{k\alpha}(\mathbf{x}, \mathbf{y})}{\partial y_\beta} \right).$$

Comparing (5.7) to (4.7), there are two additional terms in (5.7) that account for Marangoni forces and surface-viscous stresses at the contact line. Note that (5.7) assumes that the hole in the interface created by an adhered colloid is of constant surface area.

As before, we may generate a multipole expansion for $\mathbf{u}(\mathbf{x})$ by replacing \mathbf{H} , $\mathbf{T}(\mathbf{H};)$, and $\Sigma(\mathbf{H};)$ in (5.7) with their respective Taylor series in \mathbf{y} about the origin $\mathbf{0}$, which we place at an appropriate point on the interface. We may write the expansion as $\mathbf{u} = \mathbf{u}^{(1)} + \mathbf{u}^{(2)} + \mathbf{u}^{(i)}$, where

$$\mathbf{u}^{(1)} = \text{same as (4.8) with } \mathbf{G} \text{ replaced by } \mathbf{H}, \quad (5.8)$$

$$\mathbf{u}^{(2)} = \text{same as (4.9) with } \mathbf{G} \text{ replaced by } \mathbf{H}, \quad (5.9)$$

and

$$\begin{aligned} u_k^{(i)}(\mathbf{x}) = & - \sum_{n=0}^{\infty} \frac{1}{n!} \left(\int_C [\hat{m}_\alpha \varsigma_{\alpha\beta}](\mathbf{y}) y_{\gamma_1} \cdots y_{\gamma_n} dC(\mathbf{y}) \right) \frac{\partial^n H_{k\beta}(\mathbf{x}, \mathbf{y} \in I)}{\partial y_{\gamma_1} \cdots \partial y_{\gamma_n}} \Big|_{\mathbf{y}=\mathbf{0}} \\ & + \sum_{n=0}^{\infty} \frac{1}{n!} \left(\int_C [u_\beta \hat{m}_\alpha](\mathbf{y}) y_{\gamma_1} \cdots y_{\gamma_n} dC(\mathbf{y}) \right) \frac{\partial^n \Sigma_{\alpha\beta k}(\mathbf{H}; \mathbf{y} \in I, \mathbf{x})}{\partial y_{\gamma_1} \cdots \partial y_{\gamma_n}} \Big|_{\mathbf{y}=\mathbf{0}}. \end{aligned} \quad (5.10)$$

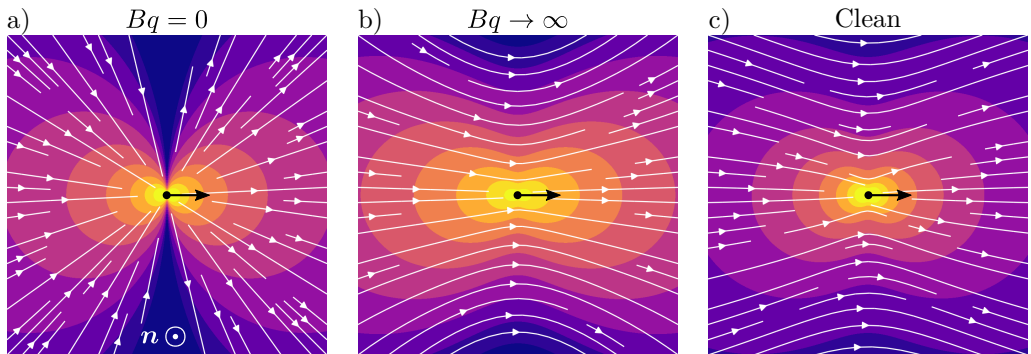


FIGURE 4. Limiting forms of the surface-incompressible monopole moment for (a) $Bq = 0$ and (b) $Bq \gg 1$ viewed on the interfacial plane $z = 0$. The direction of the point force exerted on the interfacial plane is indicated by the black arrow. The result for a clean interface (c) is also shown for comparison. Interestingly, a purely radial flow is recovered for $Bq = 0$, while the angular dependence of the clean and the large- Bq incompressible interface are similar.

Collecting terms from (5.8) to (5.10), we may write \mathbf{u} as a multipole expansion analogous to that given by (4.9),

$$\mathbf{u}(\mathbf{x}) = \mathbf{u}^{\text{m0}}(\mathbf{x}) + \mathbf{u}^{\text{m1}}(\mathbf{x}) + \text{h.o.t}, \quad (5.11)$$

where

$$u_i^{\text{m0}}(\mathbf{x}) = F_i^{(1)} H_{ij}(\mathbf{x}, \mathbf{0}^+) + F_i^{(2)} H_{ij}(\mathbf{x}, \mathbf{0}^-) + F_i^{(i)} H_{i\beta}(\mathbf{x}, \mathbf{0}) \quad (5.11a)$$

$$u_i^{\text{m1}}(\mathbf{x}) = D_{jk}^{(1)} \frac{\partial H_{ij}}{\partial y_k}(\mathbf{x}, \mathbf{0}^+) + D_{jk}^{(2)} \frac{\partial H_{ij}}{\partial y_k}(\mathbf{x}, \mathbf{0}^-) + D_{\beta\gamma}^{(i)} \frac{\partial H_{i\beta}}{\partial y_\gamma}(\mathbf{x}, \mathbf{0}). \quad (5.11b)$$

Equations (5.11a) and (5.11b) are analogous to (4.10a) and (4.10b), respectively, where (5.11a) and (5.11b) each contain an additional term to account for Marangoni and surface-viscous stresses exerted by the colloid on the interface at the contact line. While the particular functional form of the monopole and dipole moments are clearly modified by these interfacial stresses, their physical interpretation remains very similar to those found for a clean interface.

5.2.2. Monopole Moment

Compared with that for a clean interface (4.12), the monopole moment also accounts for the force exerted on the interface by the colloid at the contact line due to Marangoni and surface-viscous stresses. This force is given by the prefactor of the final term in this equation,

$$F_\beta^{(i)} = - \oint_C \hat{m}_\alpha \varsigma_{\alpha\beta} dC. \quad (5.12)$$

Again, $\mathbf{H}(\mathbf{x}, \mathbf{y})$ is continuous as \mathbf{y} is moved across the interface, so we may drop the separate limits in (5.11a) to give

$$u_i^{\text{m0}}(\mathbf{x}) = \left(F_j^{(1)} + F_j^{(2)} + F_\beta^{(i)} \delta_{\beta j}^\parallel \right) H_{ij}(\mathbf{x}, \mathbf{0}). \quad (5.13)$$

Like the clean-interface monopole, the incompressible monopole given by (4.12) does not depend on the viscosity contrast between the two fluids. Unlike the case for a clean interface, here, \mathbf{u}^{m0} does not reduce to an effective, viscosity-averaged flow due to the nontrivial interfacial dynamics. Figure 4 shows the velocity field of the monopole moment in the limits $Bq \rightarrow 0$ and $Bq \rightarrow \infty$, which are given by (5.4) and (5.6), respectively.

5.2.3. Dipole Moment

The dipole moment also has an additional contribution due to interfacial stresses given by the final term in (5.11*b*), whose prefactor is

$$D_{\beta\gamma}^{(i)} = \oint_C [\hat{m}_\alpha \varsigma_{\alpha\beta} x_\gamma + \mu_s (\hat{m}_\beta u_\gamma + u_\gamma \hat{m}_\beta)] dC. \quad (5.14)$$

Noting that only the z -component of the gradient of \mathbf{H} (with respect to \mathbf{x} or \mathbf{y}) is discontinuous across the interface, we rewrite (5.11*b*) as

$$\begin{aligned} u_i^{\text{ml}}(\mathbf{x}) = & \left(D_{\alpha\beta}^{(1)} + D_{\alpha\beta}^{(2)} + D_{\alpha\beta}^{(i)} \right) \frac{\partial H_{i\alpha}}{\partial y_\beta}(\mathbf{x}, \mathbf{0}) + D_{\alpha 3}^{(1)} \frac{\partial H_{i\alpha}}{\partial y_3}(\mathbf{x}, \mathbf{0}^+) + D_{\alpha 3}^{(2)} \frac{\partial H_{i\alpha}}{\partial y_3}(\mathbf{x}, \mathbf{0}^-) \\ & + \left(D_{3\beta}^{(1)} + D_{3\beta}^{(2)} \right) \frac{\partial H_{i3}}{\partial y_\beta}(\mathbf{x}, \mathbf{0}) + \left(D_{33}^{(1)} + D_{33}^{(2)} \right) \frac{\partial H_{i3}}{\partial y_3}(\mathbf{x}, \mathbf{0}). \end{aligned} \quad (5.15)$$

The fourth term of (5.11*b*) vanishes because $H_{i3}(\mathbf{x}, \mathbf{y})$ vanishes for $\mathbf{y} \in I$. Recall, the Green's function for a clean interface had the same property due to the non-deformability of the interface. The final term of (5.15) also vanishes; the incompressibility of the interface and the surrounding fluid, $\nabla \cdot \mathbf{u} = \nabla_s \cdot \mathbf{u} = \mathbf{0}$, implies that

$$0 = \frac{\partial H_{\alpha j}(\mathbf{x}, \mathbf{y})}{\partial x_\alpha} \Big|_{x_3=0} = \frac{\partial H_{3j}(\mathbf{x}, \mathbf{y})}{\partial x_3} \Big|_{x_3=0} = \frac{\partial H_{j3}(\mathbf{x}, \mathbf{y})}{\partial y_3} \Big|_{y_3=0}, \quad (5.16)$$

where the final equality follows from (5.2).

We may decompose $\mathbf{D}^{(1)}$ and $\mathbf{D}^{(2)}$ into irreducible tensors as before (4.14). A similar decomposition of $\mathbf{D}^{(i)}$ is

$$D_{\alpha\beta}^{(i)} = S_{\alpha\beta}^{(i)} + \frac{1}{2} \varepsilon_{\alpha\beta 3} L^{(i)} + \frac{1}{2} \delta_{\alpha\beta} D_{\gamma\gamma}^{(i)}, \quad (5.17)$$

where the irreducible part of $\mathbf{D}^{(i)}$ is

$$S_{\alpha\beta}^{(i)} = \frac{1}{2} \left(D_{\alpha\beta}^{(i)} + D_{\beta\alpha}^{(i)} \right) - \frac{1}{2} \delta_{\alpha\beta} D_{\gamma\gamma}^{(i)},$$

which represents the stresslet *on* the interface due to stresses at the contact line. Similarly, the pseudoscalar $L^{(i)}$, given by

$$L^{(i)} = -\hat{\mathbf{i}}_z \cdot \oint_C \mathbf{y} \times [\hat{\mathbf{m}} \cdot \boldsymbol{\varsigma}](\mathbf{y}) dC(\mathbf{y}), \quad (5.18)$$

is the torque (about the z axis) exerted on the interface by the colloid. The total torque exerted on the surrounding system (both fluids and the interface) is therefore $\mathbf{L} = \mathbf{L}^{(1)} + \mathbf{L}^{(2)} + L^{(i)} \hat{\mathbf{i}}_z$. Recalling the definition of $\boldsymbol{\varsigma}$ (2.6), it is readily shown that surface pressure π makes no contribution to $L^{(i)}$, and therefore $L^{(i)} = 0$ if $\mu_s = 0$. Finally, we note that applying the self-adjoint relation to the first equality in (5.16) gives $[\partial H_{j\alpha}(\mathbf{x}, \mathbf{y}) / \partial y_\alpha]_{y_3=0} = 0$. Comparing this result with (5.15) reveals that the surface traces of $\mathbf{D}^{(1)}$, $\mathbf{D}^{(2)}$, and $\mathbf{D}^{(i)}$, e.g., $\delta_{\alpha\beta} D_{\alpha\beta}^{(\nu)}$, are of no dynamical significance.

Incompressibility of the surrounding fluids further implies that $S_{33}^{(1)}$ and $S_{33}^{(2)}$ also have no affect on the flow. Recall that, for a clean interface, the modes associated with these components of the stresslet produced radially symmetric modes associated with local expansion or compression of the interface (see figure 3*b*). It is no surprise that these source/sink flows vanish for incompressible interfaces. One may easily verify that there exists no radially symmetric vector field on the interface that both satisfies $\nabla_s \cdot \mathbf{u} = 0$ and vanishes at infinity.

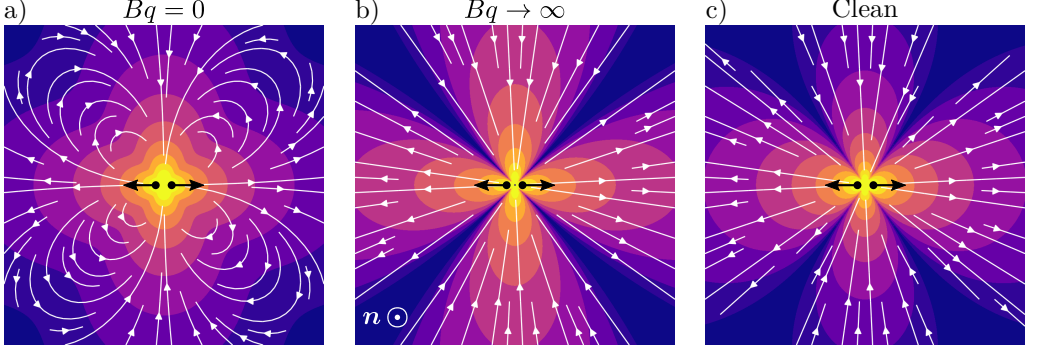


FIGURE 5. Limiting forms of the surface-incompressible stresslet (dipole moment) for (a) $Bq = 0$ and (b) $Bq \gg 1$ viewed on the interfacial plane $z = 0$. The result for a clean interface (c) is shown for comparison. The black arrows indicate the configuration of the force doublet.

After dropping all vanishing terms, (4.14) and (5.17) in (5.15) gives

$$u_i^{m1}(\mathbf{x}) = \left(S_{\alpha\beta}^{\parallel} + \frac{1}{2} \varepsilon_{\alpha\beta\gamma} L_3 \right) \frac{\partial H_{i\alpha}}{\partial y_\beta}(\mathbf{x}, \mathbf{0}) + \left(S_{l3}^{(1)} - \frac{1}{2} \varepsilon_{3lm} L_m^{(1)} \right) \frac{\partial H_{i\alpha}}{\partial y_3}(\mathbf{x}, \mathbf{0}^+) + \left(S_{l3}^{(2)} - \frac{1}{2} \varepsilon_{3lm} L_m^{(2)} \right) \frac{\partial H_{i\alpha}}{\partial y_3}(\mathbf{x}, \mathbf{0}^-), \quad (5.19)$$

where

$$S_{\alpha\beta}^{\parallel} = \left(\delta_{\alpha\gamma} \delta_{\beta\delta} - \frac{1}{2} \delta_{\alpha\beta} \delta_{\delta\gamma} \right) \left(S_{\gamma\delta}^{(1)} + S_{\gamma\delta}^{(2)} + S_{\gamma\delta}^{(i)} \right). \quad (5.20)$$

The last two terms of (5.19) are analogous to the asymmetric modes discussed for clean interfaces, given by the last two terms of (4.19). Recall that, for a clean interface, these modes have vanishing velocity on the interface. Thus, these modes are also valid for incompressible interfaces. Indeed, for $\mathbf{u}(\mathbf{x} \in I) = \mathbf{0}$, the interfacial stress balance (2.7) reduces to that for a clean interface (2.3). We also see from (5.19) that the prefactors of these modes do not involve $\mathbf{D}^{(i)}$ and therefore have no explicit dependence on the interfacial stresses. Thus, we may simply replace, without modification, the last two terms in (5.19) with the last two terms from (4.19), yielding the dipole moment as

$$u_i^{m1}(\mathbf{x}) = - \left(S_{\alpha\beta}^{\parallel} + \frac{1}{2} \varepsilon_{\alpha\beta\gamma} L_3 \right) \frac{\partial H_{i\alpha}^0}{\partial y_\beta} + \left(\frac{\mu(-z)}{\bar{\mu}\mu_1} A_{jk}^{(1)} + \frac{\mu(-z)}{\bar{\mu}\mu_2} A_{jk}^{(2)} \right) \frac{\partial J_{ij}(\mathbf{x})}{\partial x_k}, \quad (5.21)$$

where $\mathbf{A}^{(\nu)}$ is given, as before, by (4.22). In contrast, the first term of (5.21) is greatly affected by interfacial stresses. Evaluating the necessary gradient of \mathbf{H} , we find that (see appendix B)

$$\left. \frac{\partial H_{\alpha\beta}^0}{\partial y_\gamma} \right|_{\mathbf{y}=0} = - \left. \frac{\partial H_{\alpha\beta}^0}{\partial x_\gamma} \right|_{\mathbf{y}=0} = \frac{R'_1}{8\pi\bar{\mu}} (3\hat{s}_\gamma \delta_{\alpha\beta} - \hat{s}_\alpha \delta_{\beta\gamma} - \hat{s}_\beta \delta_{\gamma\alpha}) + \frac{R'_3}{2\pi\bar{\mu}} \{ \hat{s}_\alpha \hat{s}_\beta \hat{s}_\gamma \}_0, \quad (5.22)$$

where the functions $R'_n = R'_n(L_B; s, z)$ are given by (B 18).

Figure 5 shows the velocity field expressed by (5.21) in the limits $Bq \rightarrow 0$ and $Bq \rightarrow \infty$, which are given by (5.4) and (5.6), respectively. In the former limit, R'_n reduces to the closed form expression given by (B 16) and decays spatially as $1/r^2$, which is the same as the far-field behavior of the dipole moment for a clean interface. We could also obtain the result for $Bq = 0$ by evaluating the gradient of (5.4) directly. We may similarly obtain the limiting behavior for $Bq \rightarrow \infty$ as the two-dimensional Stokeslet dipole, i.e.,

the gradient of equation (5.6), which is given by

$$\left. \frac{\partial H_{\alpha\beta}^0}{\partial y_\gamma} \right|_{Bq \rightarrow \infty} \sim \frac{2\hat{s}_\alpha \hat{s}_\beta \hat{s}_\gamma - \hat{s}_\alpha \delta_{\beta\gamma} - \hat{s}_\beta \delta_{\gamma\alpha} + \hat{s}_\gamma \delta_{\alpha\beta}}{4\pi\mu_s s}. \quad (5.23)$$

The velocity field represented by (5.23) decays as $1/r$ and hence converges as $|\mathbf{s}| \rightarrow \infty$. This behavior contrasts with the monopole moment, which diverges logarithmically. However, as a three-dimensional flow, (5.23) has no z dependence and is constant in this direction, which is just another manifestation of Stokes' paradox. For Bq large but finite, the required decay of the velocity along the z direction occurs at distances $z \gtrsim L_B$. Far beyond the Boussinesq length, where $z/l \gg Bq$, the $1/r^2$ decay of an inviscid interface is (eventually) recovered.

5.3. Discussion

In the context of trapped driven and active colloids, the interpretation of the leading-order monopole and dipole moments is largely the same as that discussed for clean interfaces. However, incompressibility dramatically restructures the behavior of these hydrodynamic modes. For instance, consider the dipolar mode associated with the S_{33} component of the stresslet. At a clean interface, active colloids set up a source or sink flow on the interface (see figure 3b). These modes vanish for incompressible interfaces because the interface can no longer contract/expand to compensate for the source/sink. The remaining modes are significantly altered by surface incompressibility (see figures 4 and 5) with the exception of the asymmetric modes.

Recall that, at clean interfaces, the far-field fluid velocity both parallel and normal to the interface decays at the same rate: generally, $|\mathbf{u}| \sim r^{-1}$ for driven colloids and $|\mathbf{u}| \sim r^{-2}$ for active colloids (or colloids driven only by an external torque). If surface-viscous stresses are weak, $Bq \ll 1$, then this far-field behavior also holds for the velocity components parallel to the interface. Namely, $|\mathbf{u}^|| \sim r^{-1}$ for driven colloids and $|\mathbf{u}^|| \sim r^{-2}$ for active colloids, where $\mathbf{u}^| = \mathbf{l}_s \cdot \mathbf{u}$. However, the leading-order flow normal to the interface is significantly hindered. This hindrance is most severe for symmetric colloids, for which $\mathbf{A}^{(\nu)} = \mathbf{0}$. In this case, the monopole and dipole moments only produce flow parallel to the interface, and $u_3^{m0} = u_3^{m1} = 0$. Hence, the fluid velocity normal to the interface is generally quadrupolar to leading order and decays at least as fast as r^{-3} . For driven and active colloids trapped in an asymmetric configuration, for which $\mathbf{A}^{(\alpha)} \neq \mathbf{0}$, we recover the longer-ranged behavior $u_3 \sim r^{-2}$ associated with the dipole moment. Thus, this mode is of special importance. It may increase the rate at which colloids near the interface are transported toward or away from the interface via hydrodynamic interactions with driven or active colloids trapped at the interface. By the same mechanism, an active sheet of many trapped colloids at the interface may enhance mass transport in the z direction. If the colloids comprising the active sheet move about randomly, this enhanced transport will likely lead to active diffusion. On the other hand, directed mass transport could be accomplished through organized motion of the active sheet. These possibilities are ripe opportunities for future research.

While the flow normal to an incompressible interface is hindered in comparison to a clean interface, surface-viscous effects create very long-ranged flow parallel to the interface. Considering first the spatial behavior along the interfacial plane, we find that, for $Bq \gg 1$ and distances $s \ll L_B$ from the colloid, $\mathbf{u}^| \sim \ln s$ for the monopole moment and $\mathbf{u}^| \sim s^{-1}$ for dipole moment. This behavior is simply that of a two-dimensional Stokes flow, which is recovered in the limit of highly viscous interfaces (Saffman & Delbrück 1975). The divergent behavior of the velocity field is curtailed at distances

$s \gtrsim L_B$, where bulk-viscous effects inevitably become important. To determine the spatial behavior along the z -axis, we observe from (B 15) and (B 18) that, for $s \rightarrow 0$,

$$R_n(L_B; 0, z) \sim \frac{e^{2|z|/L_B}}{L_B} E_1\left(\frac{2|z|}{L_B}\right) \quad (5.24)$$

$$R'_n(L_B; 0, z) \sim \frac{e^{2|z|/L_B}}{L_B |z|} E_2\left(\frac{2|z|}{L_B}\right), \quad (5.25)$$

where $E_p(x) = \int_1^\infty e^{-xt}/t^p dt$ is the generalized exponential integral. We note that (Olver *et al.* 2010)

$$E_p(x) \sim \begin{cases} [(-1)^p/(p-1)!] x^{p-1} \ln x & \text{for } x \ll 1 \\ E_p(x) \sim e^{-x}/x & \text{for } x \gg 1 \text{ and for all } p, \end{cases} \quad (5.26)$$

which implies that, for $|z| \ll L_B$, $R_n \sim \ln |z|$ and $R'_n \sim \ln |z|$. Recalling that R_n and R'_n govern the spatial behavior of the monopole and dipole moments, respectively, we see that both are logarithmically divergent in z as Bq is made large. Therefore, the lamellar motion of the fluid strongly persists up to distances $z = O(L_B)$ into the surrounding fluid, regardless of whether the source of the motion is due to a driven or active colloid. At distances $z \gg L_B$, we find that $R_n \sim z^{-1}$ and $R'_n \sim z^{-2}$, so the far-field decay expected for $Bq \ll 1$ is recovered.

We expect this strong lateral fluid motion to significantly enhance spreading of a substance in directions parallel to the interface via Taylor dispersion. The shear flow driving Taylor dispersion is in this case generated by the motion of trapped colloids rather than motion of a bulk fluid relative to a no-slip boundary. The asymmetric modes that produce fluid motion normal to the interface are not modified by surface viscosity. Hence, $u_3 \sim 1/r^2$ for all Bq . Future work will examine the implications of this fluid motion on transport and mixing rates.

6. Conclusion

6.1. Summary

We have determined the leading order far-field flows generated by driven and active colloids trapped at planar fluid interfaces by a pinned contact line for $Ca \gg 1$. Under these assumptions, the colloid is trapped in a fixed configuration and cannot move perpendicular to the interface. At clean interfaces devoid of surfactant, driven colloids produce viscosity-averaged Stokeslets when driven along the interface—the flow is no different than that expected for a colloid driven in an unbounded fluid of viscosity $\bar{\mu}$. Contact-line pinning at large Ca prevents such colloids from being driven normal to the interface. Similarly, active colloids produce viscosity-averaged force dipoles (stresslets) aligned in the swimming direction, similar to those generated by a swimmer in an unbounded fluid. This stresslet is associated with balanced hydrodynamic thrust and drag in the swimming direction. However, due to pinning of the contact line, such swimmers also generate additional pumping flows that are associated with net hydrodynamic forces and torques on the colloid that are supported by the interface. Some of these modes are associated with a net hydrodynamic force or torque on the colloid, which are supported by the pinned contact line, in contrast to swimmers in the bulk phase. These modes vanish if the colloid is adjacent, rather than adhered, to the interface.

We consider surfactants, which render the interface incompressible even in the limit of scant surface concentrations. This constraint is generally applicable to driven and active

colloids which move on interfaces for $Ca \gg 1$. In this case, the flow modes associated with forced or self-propelled motion along the interface are altered significantly, even if the surfactant is dilute. An interesting feature of these modes is that they only induce lamellar fluid motion for which $u_z = 0$ at all distances z from the interface. For active colloids in particular, the pumping mode associated swimming directly against the interface (i.e., in a perpendicular configuration) is eliminated for incompressible interfaces. We also find a set of force-dipole pumping modes that induce zero velocity at the interface and therefore persist independent of the interfacial mechanics. One such mode is produced when a pinned active colloid exerts a hydrodynamic torque on the interface. These modes may be of special importance to fluid mixing near boundaries—including solid ones—as they generate fluid motion normal to the interface.

6.2. Future work and open issues

A clear direction for future work is to probe experimental systems for signatures of the flow modes reported here. The differences we predict in the flow modes induced by active colloids in the adhered states versus adjacent states may be a useful in distinguishing these two cases in experiment. While we have determined the modes expected to dominate the far-field flow for driven and active colloids based on their trapped configuration the interface, comparison of our results to experimental datasets or computational results accounting for the near-field hydrodynamic details of particular colloids would be extremely valuable.

Several open issues remain. We have not considered the effect of contact-line undulations on the flow. Interestingly, interfacial deformations due to such undulations are expected to decay at the same $1/r^2$ rate as the flow for an active colloid of negligible weight. Thus, these undulations may alter the flows we predict in interesting ways, especially because the contact line of an individual colloid may undulate randomly, being different for every colloid (Stamou *et al.* 2000; Kaz *et al.* 2012). Another use for driven and active colloids at interfaces is to enhance mixing. Enhanced mixing in active colloidal suspensions has been studied extensively in bulk fluids (Darnton *et al.* 2004; Pushkin & Yeomans 2013; Lin *et al.* 2011; Kasyap *et al.* 2014) and also in the vicinity of solid boundaries (Mathijssen *et al.* 2015; Mathijssen 2018; Kim & Breuer 2004). Different behavior is expected for mobile fluid interfaces and will vary depending on the interfacial rheology and the adhered state of the active colloids that populate the interface. Using active or driven colloids to enhance transport processes presents an untapped dimension for interfacial engineering; interfaces are natural sites for many chemical reaction and separation processes. Our work emphasizes the importance of broken symmetry in the generation of mixing by active or passive colloids at interfaces. Such asymmetry naturally arises due to defects in colloid geometry, asymmetric trapped states, and, for active colloids, differences in activity in either fluid phase. Experimentalists seeking to enhance mixing using colloids at fluid interfaces should seek to design systems that maximize these sources of asymmetry. In addition, the effect of the interface on hydrodynamic interactions between swimmers at interfaces has yet to be investigated. Finally, while we have focused on far-field flows, detailed computations of the near-field hydrodynamics of specific types of active colloids in different adhered will also yield useful information such as the predicted trajectories of such colloids.

The authors acknowledge useful discussions with Dr. Mehdi Molaei and Ms. Jiayi Deng as well as financial support from the National Science Foundation (NSF Grant No. DMR-1607878 and CBET-1943394) and the Gulf of Mexico Research Initiative. Declaration of Interests. The authors report no conflict of interest.

Appendix A. Self-adjoint property of the Green's functions

To show that the Green's function \mathbf{G} defined by (4.3) is self-adjoint, i.e., $\mathbf{G}(\mathbf{x}, \mathbf{y}) = \mathbf{G}^\top(\mathbf{y}, \mathbf{x})$, we make the following substitutions into (3.6):

$$\begin{aligned} \mathbf{u}(\mathbf{x}) &\rightarrow \mathbf{G}(\mathbf{x}, \mathbf{y}) \cdot \mathbf{F}, & \mathbf{u}'(\mathbf{x}) &\rightarrow \mathbf{G}(\mathbf{x}, \mathbf{y}') \cdot \mathbf{F}', \\ \boldsymbol{\sigma}(\mathbf{x}) &\rightarrow \mathbf{T}(\mathbf{G}; \mathbf{x}, \mathbf{y}) \cdot \mathbf{F}, & \boldsymbol{\sigma}'(\mathbf{x}) &\rightarrow \mathbf{T}(\mathbf{G}; \mathbf{x}, \mathbf{y}') \cdot \mathbf{F}', \\ \mathbf{f}(\mathbf{x}) &\rightarrow -\mathbf{F}\delta_{\mathbb{R}^3}(\mathbf{x} - \mathbf{y}), & \mathbf{f}'(\mathbf{x}) &\rightarrow -\mathbf{F}\delta_{\mathbb{R}^3}(\mathbf{x} - \mathbf{y}'), \\ \mathbf{f}_s(\mathbf{x}) &\rightarrow -\mathbf{F}\delta_{\mathbb{R}^2}(\mathbf{x} - \mathbf{y}), & \mathbf{f}'_s(\mathbf{x}) &\rightarrow -\mathbf{F}\delta_{\mathbb{R}^2}(\mathbf{x} - \mathbf{y}'). \end{aligned} \quad (\text{A } 1)$$

That is, we choose \mathbf{u} as the flow field due to a point force \mathbf{F} at \mathbf{y} and \mathbf{u}' the flow field due to another point force \mathbf{F}' at point \mathbf{y}' . The point forces and their locations are arbitrary and may be exerted on either fluid or the interface. Each fluid domain is semi-infinite and bounded only by the interface. With the above substitutions, (3.6) becomes

$$\begin{aligned} 0 &= \int_{V^*} [\delta_{\mathbb{R}^3}(\mathbf{x} - \mathbf{y}) \mathbf{F} \cdot \mathbf{G}(\mathbf{x}, \mathbf{y}') \cdot \mathbf{F}' - \delta_{\mathbb{R}^3}(\mathbf{x} - \mathbf{y}') \mathbf{F}' \cdot \mathbf{G}(\mathbf{x}, \mathbf{y}) \cdot \mathbf{F}] \, dV \\ &\quad + \int_{I^*} [\delta_{\mathbb{R}^2}(\mathbf{x} - \mathbf{y}) \mathbf{F} \cdot \mathbf{G}(\mathbf{x}, \mathbf{y}') \cdot \mathbf{F}' - \delta_{\mathbb{R}^2}(\mathbf{x} - \mathbf{y}') \mathbf{F}' \cdot \mathbf{G}(\mathbf{x}, \mathbf{y}) \cdot \mathbf{F}] \, dA \\ &\quad + \oint_R \{ [\mathbf{T}(\mathbf{x}, \mathbf{y}) \cdot \mathbf{F}] \cdot [\mathbf{G}(\mathbf{x}, \mathbf{y}') \cdot \mathbf{F}'] - [\mathbf{T}(\mathbf{x}, \mathbf{y}') \cdot \mathbf{F}'] \cdot [\mathbf{G}(\mathbf{x}, \mathbf{y}) \cdot \mathbf{F}] \} \cdot \hat{\mathbf{n}} \, dS, \end{aligned} \quad (\text{A } 2)$$

where, for brevity, we omit \mathbf{G} as an argument to \mathbf{T} . The integrations in (A 2) are taken to be over an arbitrary volume that may contain points on the interface. If the boundaries of this volume in each fluid, represented by R , are made arbitrarily far from the points \mathbf{y} and \mathbf{y}' , then the final integral in (A 2) vanishes; $\mathbf{G} \sim r^{-1}$ and $\mathbf{T}(\mathbf{G};) \sim 1/r^{-2}$, so this integral decays as L_V^{-1} as $L_V \rightarrow \infty$, where L_V is the characteristic size of the integration region. Then, using the definition of the Dirac delta, (A 2) simplifies to

$$\mathbf{F} \cdot \mathbf{G}(\mathbf{y}, \mathbf{y}') \cdot \mathbf{F}' = \mathbf{F}' \cdot \mathbf{G}(\mathbf{y}', \mathbf{y}) \cdot \mathbf{F}. \quad (\text{A } 3)$$

Since \mathbf{F} , \mathbf{F}' , \mathbf{y} , and \mathbf{y}' are all arbitrary, (A 3) implies that $\mathbf{G}(\mathbf{y}, \mathbf{y}') = \mathbf{G}^\top(\mathbf{y}', \mathbf{y})$, that is, \mathbf{G} is self-adjoint.

Using the same procedure, it may be shown that \mathbf{H} is also self-adjoint. Making a set of substitutions analogous to those appearing in (A 1) along with the additional substitutions $\boldsymbol{\varsigma}(\mathbf{x}) \rightarrow \boldsymbol{\Sigma}(\mathbf{H}; \mathbf{x}, \mathbf{y}) \cdot \mathbf{F}$ and $\boldsymbol{\varsigma}(\mathbf{x}) \rightarrow \boldsymbol{\Sigma}(\mathbf{H}; \mathbf{x}, \mathbf{y}') \cdot \mathbf{F}'$ into (3.8), we find

$$\begin{aligned} 0 &= \mathbf{F}' \cdot \mathbf{H}(\mathbf{y}', \mathbf{y}) \cdot \mathbf{F} - \mathbf{F} \cdot \mathbf{H}(\mathbf{y}, \mathbf{y}') \cdot \mathbf{F}' \\ &\quad + \oint_R \{ [\mathbf{T}(\mathbf{x}, \mathbf{y}) \cdot \mathbf{F}] \cdot [\mathbf{H}(\mathbf{x}, \mathbf{y}') \cdot \mathbf{F}'] - [\mathbf{T}(\mathbf{x}, \mathbf{y}') \cdot \mathbf{F}'] \cdot [\mathbf{H}(\mathbf{x}, \mathbf{y}) \cdot \mathbf{F}] \} \cdot \hat{\mathbf{n}} \, dS \\ &\quad + \oint_{\partial I^*} \{ [\boldsymbol{\Sigma}(\mathbf{x}, \mathbf{y}) \cdot \mathbf{F}] \cdot [\mathbf{H}(\mathbf{x}, \mathbf{y}') \cdot \mathbf{F}'] - [\boldsymbol{\Sigma}(\mathbf{x}, \mathbf{y}') \cdot \mathbf{F}'] \cdot [\mathbf{H}(\mathbf{x}, \mathbf{y}) \cdot \mathbf{F}] \} \cdot \hat{\mathbf{m}} \, dC. \end{aligned} \quad (\text{A } 4)$$

In this case, an additional integral over ∂I^* appears, which is the curve where our arbitrarily chosen fluid region intersects the interface. Both integrals in (A 4) vanish as $L_V \rightarrow \infty$ provided that the Boussinesq length L_B remains finite. For $r \gg L_B$, \mathbf{H} and \mathbf{G} share the same far-field decay behavior, i.e., $\mathbf{H} \sim r^{-1}$. From the remaining two terms in (A 4), we find $\mathbf{H}(\mathbf{y}, \mathbf{y}') = \mathbf{H}^\top(\mathbf{y}', \mathbf{y})$.

Appendix B. Computation of the Green's functions

Here, we derive the Green's functions \mathbf{G} and \mathbf{H} used in sections 4 and 5, respectively. Consider two immiscible fluids separated by a planar interface on the $z = 0$ plane with a

point force \mathbf{f} applied at the point $(0, 0, h)$. Let $\widehat{f}(\mathbf{k}) = \iint_{\mathbb{R}^2} f(\mathbf{x}^{\parallel}) \exp[-i\mathbf{k} \cdot \mathbf{s}] d^2\mathbf{s}$ define the two-dimensional Fourier transform of $f(\mathbf{s})$ in the x - y plane, where $\mathbf{s} = (x, y)$ is the position vector on the interface. It is convenient to start with the boundary integral form of the Stokes equations for the upper and lower fluids, which, after applying the Fourier transform, are

$$\mathbb{I}_{z>0} \widehat{u}_i^1(\mathbf{k}, z) = -\widehat{T}_{3\alpha i}(\mathbf{J}; \mathbf{k}, z) \widehat{v}_\alpha(\mathbf{k}) - \frac{1}{\mu_1} \widehat{J}_{ij}(\mathbf{k}, z) \widehat{t}_j^1(\mathbf{k}) + \frac{\mathbb{I}_{h>0}}{\mu_1} \widehat{J}_{ij}(\mathbf{k}, z-h) f_j \quad (\text{B1})$$

$$\mathbb{I}_{z<0} \widehat{u}_i^2(\mathbf{k}, z) = \widehat{T}_{3\alpha i}(\mathbf{J}; \mathbf{k}, z) \widehat{v}_\alpha(\mathbf{k}) + \frac{1}{\mu_2} \widehat{J}_{ij}(\mathbf{k}, z) \widehat{t}_j^2(\mathbf{k}) + \frac{\mathbb{I}_{h<0}}{\mu_2} \widehat{J}_{ij}(\mathbf{k}, z-h) f_j, \quad (\text{B2})$$

respectively, where $J_{ij} = (\delta_{ij}/r + x_i x_j/r^3)/8\pi$ is the Oseen tensor, $T_{ijk}(\mathbf{J};) = -\delta_{ij} P_k(\mathbf{J};) + (\nabla_i J_{jk} - \nabla_j J_{ik})$, $\mathbf{t}^\nu = \hat{\mathbf{i}}_z \cdot \boldsymbol{\sigma}^\nu$ is the surface traction at the interface, and $\mathbf{v}(\mathbf{s}) = \mathbf{u}(\mathbf{s}, z=0)$ is the surface velocity on the interface. For notational convenience, we hereafter omit \mathbf{J} as an argument to \mathbf{T} . The Fourier transform of \mathbf{J} is given by

$$\widehat{J}_{ij}(\mathbf{k}, z) = \frac{\delta_{ij}}{2k} e^{-k|z|} + \frac{1}{4k^3} \widehat{\nabla}_i \widehat{\nabla}_j \left[(1+k|z|) e^{-k|z|} \right]. \quad (\text{B3})$$

where $\widehat{\nabla}_i = ik_i + \delta_{i3}(\partial/\partial z)$.

The interface, located at $z=0$, obeys the kinematic conditions $\hat{\mathbf{i}}_z \cdot \mathbf{v} = 0$ (no flux) and $\mathbf{u}^1 = \mathbf{u}^2 = \mathbf{v}$ (continuity of velocity). These are accompanied by the dynamic condition given by the tangential stress balance at the interface, which in Fourier space is

$$\mathbf{l}_s \cdot (\widehat{\mathbf{t}}]_I + \mathbb{I}_{h=0} \mathbf{f}) = \mathbf{0} \quad (\text{B4})$$

for a clean interface and for an incompressible interface is

$$\mathbf{l}_s \cdot (\widehat{\mathbf{t}}]_I + \mathbb{I}_{h=0} \mathbf{f}) = ik\widehat{\pi} + \mu_s k^2 \widehat{\mathbf{v}}; \quad i\mathbf{k} \cdot \mathbf{v} = 0, \quad (\text{B5})$$

where $k = |\mathbf{k}|$.

Multiplying (B1) and (B2) by μ_1 and μ_2 , resp., taking the limit as $z \rightarrow 0^\pm$, resp., and adding the results gives

$$2\bar{\mu} \delta_{i\beta} \widehat{v}_\beta(\mathbf{k}) + \left(\mu_1 \lim_{z \rightarrow 0^+} - \mu_2 \lim_{z \rightarrow 0^-} \right) \widehat{T}_{3\alpha i}(\mathbf{k}, z) \widehat{v}_\alpha(\mathbf{k}) + \widehat{J}_{ij}(\mathbf{k}, 0) [\widehat{t}_j]_I(\mathbf{k}) = \widehat{J}_{ij}(\mathbf{k}, -h) f_j, \quad (\text{B6})$$

where $\bar{\mu} = (\mu_1 + \mu_2)/2$ is the average viscosity. Using (B3) and the definition of \mathbf{T} , we find that the second term on the left-hand side of (B6) reduces to

$$\lim_{z \rightarrow 0^\pm} \widehat{T}_{3\alpha i} \widehat{v}_\alpha = - \left(\pm \frac{\delta_{i\alpha}}{2} + \delta_{i3} \frac{ik_\alpha}{2k} \right) \widehat{v}_\alpha, \quad (\text{B7})$$

which is the Stokes double-layer density for either side of the interface. For a clean interface, (B4) and (B7) in (B6) yields, after a trivial Fourier inversion,

$$\bar{\mu} \mathbf{v}(\mathbf{s}) = \mathbf{l}_s \cdot \mathbf{J}(\mathbf{s} - h\hat{\mathbf{i}}_3) \cdot \mathbf{f}, \quad (\text{B8})$$

which shows that the fluid velocity at the interface is independent of the viscosity contrast and simply corresponds to the projection of the Oseen tensor, shifted to $z=h$, onto the interface at $z=0$.

We may do the same for an incompressible interface by instead using (B5) in (B6), from which we obtain

$$\left(\bar{\mu} + \frac{1}{2} \mu_s k \right) \widehat{v}_\alpha + \frac{ik_\alpha}{4k} \pi = \widehat{J}_{\alpha j}|_{z=-h} f_j. \quad (\text{B9})$$

Taking the inner product of (B 9) with $i\mathbf{k}$ and solving for π yields

$$\begin{aligned}\hat{\pi}(\mathbf{k}) &= -\frac{4}{k} i\mathbf{k} \cdot \hat{\mathbf{J}}(\mathbf{k}, -h) \cdot \mathbf{f} \\ &= \frac{e^{-k|h|}}{k^2} [(k|h| - 1)i\mathbf{k} + k^2 h \hat{\mathbf{z}}] \cdot \mathbf{f}.\end{aligned}\quad (\text{B } 10)$$

The surface pressure is associated only with the Marangoni effect and depends neither on the bulk nor surface shear viscosities. Letting $\pi(\mathbf{s}, h) = \boldsymbol{\Pi}(\mathbf{s}, h) \cdot \mathbf{f}$ and carrying out the Fourier inversion to real space, we obtain

$$\boldsymbol{\Pi}(\mathbf{s}, h) = |h| \left(\nabla_s - \hat{\mathbf{z}} \frac{\partial}{\partial h} \right) \frac{1}{4\pi\sqrt{s^2 + h^2}} + \frac{\mathbf{s}}{4\pi s^2} \left(1 - \frac{|h|}{\sqrt{s^2 + h^2}} \right), \quad (\text{B } 11)$$

where $s = |\mathbf{s}|$. For $h = 0$, this result reduces to $\boldsymbol{\Pi}(\mathbf{s}, 0) = \mathbf{s}/4\pi s^2$.

Noting that $\mathbf{v}(\mathbf{s}) \equiv \mathbf{H}(\mathbf{x} \in I, \mathbf{y}) \cdot \mathbf{f}$ for $\mathbf{y} = (0, 0, h)$, putting (B 10) in (B 9) and solving for $\hat{\mathbf{v}}$ yields

$$\begin{aligned}\hat{\mathbf{H}}(\mathbf{k}, z = 0, h) &= \frac{2}{2\bar{\mu} + \mu_s k} \left(\mathbf{I}_s - \frac{\mathbf{k}\mathbf{k}}{k^2} \right) \cdot \hat{\mathbf{J}}(\mathbf{k}, -h) \\ &= \frac{e^{-k|h|}}{2\bar{\mu} + \mu_s k} \left(\frac{\mathbf{I}_s}{k} - \frac{\mathbf{k}\mathbf{k}}{k^3} \right).\end{aligned}\quad (\text{B } 12)$$

Surface incompressibility of (B 12) is easily verified by contracting the right-hand side of this equation with $i\mathbf{k}$, thereby taking the divergence in Fourier space, which vanishes. We also see from (B 12) that a force perpendicular to the interface generates no interfacial flow; $H_{i3}(\mathbf{x} \in I, h) = 0$. We therefore conclude that the flow due to the z -component of the force is therefore the same as that for a rigid, no-slip wall, as is also noted by Bławdziewicz *et al.* (1999).

Now, the self-adjoint property of \mathbf{H} (see appendix A) permits us to swap the roles of h and z in (B 12);

$$\hat{\mathbf{H}}(\mathbf{k}, z, h = 0) = \frac{e^{-k|z|}}{2\bar{\mu} + \mu_s k} \left(\frac{\mathbf{I}_s}{k} - \frac{\mathbf{k}\mathbf{k}}{k^3} \right). \quad (\text{B } 13)$$

Remarkably, from the interfacial flow profile due to a point force at $z = h$ (B 12), we automatically obtain the flow *at all points* \mathbf{x} due to a point force at the interface ($h = 0$). Fourier inversion of (B 13) to real space gives equation (5.3),

$$H_{\alpha\beta}^0(L_B; \mathbf{x}) = \frac{1}{4\pi\bar{\mu}} R_0(L_B; s, z) \delta_{\alpha\beta} + \frac{1}{2\pi\bar{\mu}} R_2(L_B; s, z) \{ \hat{s}_\alpha \hat{s}_\beta \}_0. \quad (\text{B } 14)$$

The functions R_n are given by

$$R_n(L_B; s, z) = \int_0^\infty \frac{e^{-k|z|}}{2 + L_B k} J_n(ks) dk, \quad (\text{B } 15)$$

where J_n is the Bessel function of the first kind of order n . In the special case that $L_B = 0$, we obtain R_n in closed form as

$$R_n = \frac{(r - |z|)^n}{2rs^n}. \quad (\text{B } 16)$$

To obtain (surface) gradients of (B 14), we may take the tensor product of (B 13) with \mathbf{k} and repeat the Fourier inversion process to give

$$\frac{\partial H_{\alpha\beta}^0}{\partial x_\gamma} = \frac{\partial H_{\alpha\beta}^0}{\partial s_\gamma} = \frac{R'_1}{8\pi\bar{\mu}} (\hat{s}_\alpha \delta_{\beta\gamma} + \hat{s}_\beta \delta_{\gamma\alpha} - 3\hat{s}_\gamma \delta_{\alpha\beta}) - \frac{R'_3}{2\pi\bar{\mu}} \{ \hat{s}_\alpha \hat{s}_\beta \hat{s}_\gamma \}_0, \quad (\text{B } 17)$$

where

$$R_n(L_B; s, z) = \int_0^\infty \frac{ke^{-k|z|}}{2 + L_B k} J_n(ks) dk. \quad (\text{B } 18)$$

For $L_B = 0$, R'_n reduces to

$$R'_n = \frac{s^n(nr + |z|)}{2r^3(r + |z|)^n}. \quad (\text{B } 19)$$

To determine the full flow fields for $h \neq 0$, we can directly sum (B 1) and (B 2) to eliminate the Stokes double layer, which gives

$$\hat{u}_i(\mathbf{k}, z; h) = -\frac{1}{\bar{\mu}} \hat{J}_{ij}(\mathbf{k}, z) \hat{q}_j(\mathbf{k}; h) + \frac{1}{\mu(h)} \hat{J}_{ij}(\mathbf{k}, z - h) f_j \quad (\text{B } 20)$$

where

$$\hat{\mathbf{q}}(\mathbf{k}; h) := \bar{\mu} \left[\frac{\hat{\mathbf{t}}^1(\mathbf{k})}{\mu_1} - \frac{\hat{\mathbf{t}}^2(\mathbf{k})}{\mu_2} \right] = \bar{\mu} \left[\frac{\hat{\boldsymbol{\sigma}}(\mathbf{k}) \cdot \mathbf{n}}{\mu} \right]_I \quad (\text{B } 21)$$

is the Stokes single-layer density (in Fourier space). For a clean interface, setting $z = 0$ in (B 20) and putting (B 8) into the result yields

$$\hat{\mathbf{q}}(\mathbf{k}; h) = 4k \left(\mathbf{I} - \frac{\mu(h)}{\bar{\mu}} \mathbf{I}_s \right) \cdot \hat{\mathbf{J}}(\mathbf{k}, -h) \cdot \mathbf{f}. \quad (\text{B } 22)$$

After inserting (B 22) back into (B 20), lengthy algebraic manipulation, followed by inversion to real space, yields the velocity field in terms of the hydrodynamic image system described by $\mathbf{G} \cdot \mathbf{f}$ (4.3). A similar procedure could be used to determine $\mathbf{H}(\mathbf{x}, \mathbf{y})$ for all \mathbf{y} , but we do not require that result in this paper. Others have performed such computations of \mathbf{H} via other approaches (Bławdziewicz *et al.* 1999; Fischer *et al.* 2006).

REFERENCES

- ADEROGBA, K. & BLAKE, J. R. 1978 Action of a force near the planar surface between two semi-infinite immiscible liquids at very low Reynolds numbers. *Bulletin of the Australian Mathematical Society* **18** (3), 345–356.
- AHMADZADEGAN, ADIB, WANG, SHIYAN, VLACHOS, PAVLOS P. & ARDEKANI, AREZOO M. 2019 Hydrodynamic attraction of bacteria to gas and liquid interfaces. *Physical Review E* **100** (6), 062605.
- BŁAWDZIEWICZ, JERZY, CRISTINI, VITTORIO & LOEWENBERG, MICHAEL 1999 Stokes flow in the presence of a planar interface covered with incompressible surfactant. *Physics of Fluids* **11** (2), 251–258.
- BONIELLO, GIUSEPPE, BLANC, CHRISTOPHE, FEDORENKO, DENYS, MEDFAI, MAYSSA, MBAREK, NADIA BEN, IN, MARTIN, GROSS, MICHEL, STOCCO, ANTONIO & NOBILI, MAURIZIO 2015 Brownian diffusion of a partially wetted colloid. *Nature Materials* **14** (9), 908–911, number: 9 Publisher: Nature Publishing Group.
- DARNTON, NICHOLAS, TURNER, LINDA, BREUER, KENNETH & BERG, HOWARD C. 2004 Moving Fluid with Bacterial Carpets. *Biophysical Journal* **86** (3), 1863–1870.
- DENG, JIAYI, MOLAEI, MEHDI, CHISHOLM, NICHOLAS G. & STEBE, KATHLEEN J. 2020 Motile Bacteria at Oil–Water Interfaces: *Pseudomonas aeruginosa*. *Langmuir* Publisher: American Chemical Society.
- DESAI, NIKHIL, SHAIK, VASEEM A. & ARDEKANI, AREZOO M. 2018 Hydrodynamics-mediated trapping of micro-swimmers near drops. *Soft Matter* **14** (2), 264–278.
- DHAR, P., FISCHER, TH. M., WANG, Y., MALLOUK, T. E., PAXTON, W. F. & SEN, A. 2006 Autonomously Moving Nanorods at a Viscous Interface. *Nano Letters* **6** (1), 66–72.
- DI LEONARDO, R., DELL’ARCIPIRETE, D., ANGELANI, L. & IEBBA, V. 2011 Swimming with an image. *Physical Review Letters* **106** (3), 038101.

- DÖRR, AARON & HARDT, STEFFEN 2015 Driven particles at fluid interfaces acting as capillary dipoles. *Journal of Fluid Mechanics* **770**, 5–26, publisher: Cambridge University Press.
- DÖRR, AARON, HARDT, STEFFEN, MASOUD, HASSAN & STONE, HOWARD A. 2016 Drag and diffusion coefficients of a spherical particle attached to a fluid–fluid interface. *Journal of Fluid Mechanics* **790**, 607–618.
- ELFRING, GWYNN J., LEAL, L. GARY & SQUIRES, TODD M. 2016 Surface viscosity and Marangoni stresses at surfactant laden interfaces. *Journal of Fluid Mechanics* **792**, 712–739.
- FISCHER, TH M. 2004 The drag on needles moving in a Langmuir monolayer. *Journal of Fluid Mechanics* **498**, 123–137.
- FISCHER, TH. M., DHAR, P. & HEINIG, P. 2006 The viscous drag of spheres and filaments moving in membranes or monolayers. *Journal of Fluid Mechanics* **558**, 451.
- GIACCHÉ, DAVIDE, ISHIKAWA, TAKUJI & YAMAGUCHI, TAKAMI 2010 Hydrodynamic entrapment of bacteria swimming near a solid surface. *Physical Review E* **82** (5), 056309.
- HUGHES, B. D., PAILTHORPE, B. A. & WHITE, L. R. 1981 The translational and rotational drag on a cylinder moving in a membrane. *Journal of Fluid Mechanics* **110**, 349–372, publisher: Cambridge University Press.
- KASYAP, T. V., KOCH, DONALD L. & WU, MINGMING 2014 Hydrodynamic tracer diffusion in suspensions of swimming bacteria. *Physics of Fluids* **26** (8), 081901.
- KAZ, DAVID M., MCGORTY, RYAN, MANI, MADHAV, BRENNER, MICHAEL P. & MANOHARAN, VINOTHAN N. 2012 Physical ageing of the contact line on colloidal particles at liquid interfaces. *Nature Materials* **11** (2), 138–142.
- KIM, MIN JUN & BREUER, KENNETH S. 2004 Enhanced diffusion due to motile bacteria. *Physics of Fluids* **16** (9), L78–L81.
- KIM, SANGTAE & KARRILA, SEPPO J. 1991 *Microhydrodynamics: principles and selected applications*. Butterworth-Heinemann.
- LAUGA, ERIC, DiLUZIO, WILLOW R., WHITESIDES, GEORGE M. & STONE, HOWARD A. 2006 Swimming in Circles: Motion of Bacteria near Solid Boundaries. *Biophysical Journal* **90** (2), 400–412.
- LAUGA, ERIC & POWERS, THOMAS R. 2009 The hydrodynamics of swimming microorganisms. *Reports on Progress in Physics* **72** (9), 096601.
- LEVINE, ALEX J. & MACKINTOSH, F. C. 2002 Dynamics of viscoelastic membranes. *Physical Review E* **66** (6), 061606.
- LIN, ZHI, THIFFEAULT, JEAN-LUC & CHILDRESS, STEPHEN 2011 Stirring by squirmers. *Journal of Fluid Mechanics* **669**, 167–177.
- LOPEZ, DIEGO & LAUGA, ERIC 2014 Dynamics of swimming bacteria at complex interfaces. *Physics of Fluids* **26** (7), 071902.
- MALGARETTI, P., POPESCU, M. N. & DIETRICH, S. 2016 Active colloids at fluid interfaces. *Soft Matter* **12** (17), 4007–4023.
- MATHIJSEN, ARNOLD J. T. M. 2018 Nutrient Transport Driven by Microbial Active Carpets. *Physical Review Letters* **121** (24).
- MATHIJSEN, A. J. T. M., PUSHKIN, D. O. & YEOMANS, J. M. 2015 Tracer trajectories and displacement due to a micro-swimmer near a surface. *Journal of Fluid Mechanics* **773** (2015), 498–519.
- OLVER, FRANK W. J., LOZIER, DANIEL W., BOISVERT, RONALD F. & CLARK, CHARLES W., ed. 2010 *NIST handbook of mathematical functions*. Cambridge ; New York: Cambridge University Press : NIST, oCLC: ocn502037224.
- PIMPONI, D., CHINAPPI, M., GUALTIERI, P. & CASCIOLA, C. M. 2016 Hydrodynamics of flagellated microswimmers near free-slip interfaces. *Journal of Fluid Mechanics* **789**, 514–533.
- POZRIKIDIS, C. 2007 Particle motion near and inside an interface. *Journal of Fluid Mechanics* **575**, 333–357.
- PUSHKIN, DMITRI O. & YEOMANS, JULIA M. 2013 Fluid Mixing by Curved Trajectories of Microswimmers. *Physical Review Letters* **111** (18), 188101.
- RANGER, K. B. 1978 The circular disk straddling the interface of a two-phase flow. *International Journal of Multiphase Flow* **4** (3), 263–277.

- SAFFMAN, P. G. & DELBRÜCK, M. 1975 Brownian motion in biological membranes. *Proceedings of the National Academy of Sciences* **72** (8), 3111–3113.
- SHAIK, VASEEM A. & ARDEKANI, AREZOO M. 2017 Motion of a model swimmer near a weakly deforming interface. *Journal of Fluid Mechanics* **824**, 42–73.
- SICKERT, M., RONDELEZ, F. & STONE, H. A. 2007 Single-particle Brownian dynamics for characterizing the rheology of fluid Langmuir monolayers. *Europhysics Letters (EPL)* **79** (6), 66005.
- SPAGNOLIE, SAVERIO E. & LAUGA, ERIC 2012 Hydrodynamics of self-propulsion near a boundary: predictions and accuracy of far-field approximations. *Journal of Fluid Mechanics* **700**, 105–147.
- STAMOU, DIMITRIS, DUSCHL, CLAUS & JOHANNSMANN, DIETHELM 2000 Long-range attraction between colloidal spheres at the air-water interface: The consequence of an irregular meniscus. *Physical Review E* **62** (4), 5263–5272, publisher: American Physical Society.
- STONE, HOWARD A. & AJDARI, ARMAND 1998 Hydrodynamics of particles embedded in a flat surfactant layer overlying a subphase of finite depth. *Journal of Fluid Mechanics* **369**, 151–173, publisher: Cambridge University Press.
- STONE, HOWARD A. & MASOUD, HASSAN 2015 Mobility of membrane-trapped particles. *Journal of Fluid Mechanics* **781**, 494–505.
- VACCARI, LIANA, MOLAEI, MEHDI, L. LEHENY, ROBERT & J. STEBE, KATHLEEN 2018 Cargo carrying bacteria at interfaces. *Soft Matter* **14** (27), 5643–5653.
- WANG, XIAOLU, IN, MARTIN, BLANC, CHRISTOPHE, WÜRGER, ALOIS, NOBILI, MAURIZIO & STOCCO, ANTONIO 2017 Janus Colloids Actively Rotating on the Surface of Water. *Langmuir* **33** (48), 13766–13773.